

**Dam Foundation Erosion Study Team**

---

# **Dam Foundation Erosion**

**Phase III - Clear Water Experiments  
1:3 Scale Model Facility**

**Plunge Pool Circulation at Dam Foundations**

**Study Team Leader:  
Rodney J. Wittler**

**Scale Model Team Leader:  
Steven R. Abt**

**Principal Investigator:  
Kyle J. Hamilton**

**June 1997**

**PLUNGE POOL CIRCULATION  
AT DAM FOUNDATIONS**

Submitted to:

U.S. Bureau of Reclamation  
Reclamation Service Center  
Denver Federal Center  
Denver, Colorado 80225

Prepared by:

Kyle J. Hamilton and Steven R. Abt

Department of Civil Engineering  
Colorado State University  
Ft. Collins, Colorado 80523

May 1997

## EXECUTIVE SUMMARY

Overtopping arch dams produce a plunging jet that has the potential to erode the foundation and abutment areas at the dam base. It is important to understand the flow patterns (i.e., circulation) in the plunge pool in the region between the downstream dam face and the jet impact location to ascertain dam stability. A method was sought to predict the circulation pattern and velocities in the plunge pool basin along the downstream face of the dam and along the plunge pool basin upstream of jet impact.

A physical model was constructed in the Hydraulics Laboratory at Colorado State University to simulate a free falling, turbulent rectangular jet that impacts the free surface plunge pool resulting from overtopping. A test program was conducted varying the discharge, tailwater depth, and plunge pool basin width. The circulation patterns in the plunge pool as well as the velocity components of flow were measured and documented.

The circulation in the plunge pool between the upstream boundary and the upstream side of the jet at impact was counter-clockwise (downstream flow being left to right). The driving circulation forces are the rebound effect of the plunging jet off of the stagnation point in the plunge pool, the buoyancy force due to the air entrainment, and the horizontal spreading force due to the impact of the jet with the free surface. Velocities along the upstream face and along the basin floor were determined to be a function of the velocity at impact, air concentration at impact, plunge pool depth, the ratio of the basin width to jet width, and gravitational acceleration. The circulation velocities were found to

be approximately 10 percent of the jet impact velocities. A procedure for predicting the maximum and average velocity components along the dam toe and plunge pool base were developed.

## **FORWARD**

This study was funded through Cooperative Agreement 1425-5-FC-81-20350 between the U.S. Bureau of Reclamation and Colorado State University. Funding and technical partners in the multi year research study include Pacific Gas & Electric Company, The Electric Power Research Institute, the Reclamation Water Technology and Environmental Research Program, the Department of the Interior Dam Safety Program, Western Area Power Administration, Federal Energy Power Commission, Golder Associates, Inc., and Colorado State University.

## UNITS CONVERSIONS

Multiply number of	by	to obtain
in.	25.4	m m
in.	0.0254	m
ft	0.3048	m
ft <sup>2</sup>	0.0929	m <sup>2</sup>
in. <sup>2</sup>	6.452E-04	m <sup>2</sup>
ft <sup>3</sup>	0.02832	m <sup>3</sup>
in <sup>3</sup>	1.64E-05	m <sup>3</sup>
U.S. gallon	3.785E-03	m <sup>3</sup>
ft/s	0.3048	m/s
ft <sup>3</sup> /s	0.02832	m <sup>3</sup> /s
gpm	6.309E-05	m <sup>3</sup> /s
lbf	4.448	N
ft-lbf	1.356	N*m
slug	14.59	kg
slug/ft <sup>3</sup>	515.4	kg/m <sup>3</sup>
lbf/ft <sup>2</sup>	47.88	N/m <sup>2</sup>
lbf/in. <sup>2</sup>	6895	N/m <sup>2</sup>
lbf/ft <sup>3</sup>	157.1	N/m <sup>3</sup>
ft <sup>2</sup> /s	0.0929	m <sup>2</sup> /s
lbf-s/ft <sup>2</sup>	47.88	N*s/m <sup>2</sup>

## TABLE OF CONTENTS

<b>CHAPTER 1</b> .....	<b>1</b>
<b>CHAPTER 2</b> .....	<b>4</b>
2.1 IMPACT VELOCITY OF A FREE FALLING JET .....	4
2.2 JETS CONFINED BY BOUNDARIES.....	5
2.3.1 COLA.....	8
2.3.2 LENCASTRE .....	9
2.3.3 IAMANDI AND ROUSE.....	10
2.3.4 LEE AND JIRKA .....	12
2.3.5 JIRKA AND HARLEMAN.....	14
<b>CHAPTER 3</b> .....	<b>17</b>
3.1 LOCATION OF TEST FACILITY .....	17
3.2 MODEL DESCRIPTION .....	17
3.3 INSTRUMENTATION.....	22
3.3.1 ORIFICE PLATE.....	22
3.3.2 BACK-FLUSHING PITOT TUBE .....	23
3.3.3 AIR CONCENTRATION PROBE.....	25
3.3.4 ACOUSTIC DOPPLER VELOCIMETER .....	28
3.3.5 MARSH-McBIRNEY® VELOCITY METER.....	30
3.4 COORDINATE SYSTEM .....	30
3.5 TESTING MATRIX.....	31
3.6 TESTING PROCEDURES.....	32
<b>CHAPTER 4</b> .....	<b>36</b>
4.1 DATA REDUCTION .....	36
4.2 FLOW PATTERNS .....	37
4.3 VELOCITY PREDICTION EQUATIONS .....	42
4.3.1 VELOCITY COMPONENT AND VECTOR COMPARISON .....	43
4.3.2 DIMENSIONAL ANALYSIS.....	43
4.3.3 CRITICAL ZONES.....	45
4.3.4 DATA ANALYSIS.....	47
4.3.5 REGRESSION ANALYSIS .....	48
4.3.6 VELOCITY COMPARISONS .....	62
4.4 SPURIOUS CORRELATION ANALYSIS .....	65
4.5 EROSION POTENTIAL .....	66
<b>CHAPTER 5</b> .....	<b>68</b>

5.1 APPLICABILITY .....	68
5.2 IMPLEMENTING THE VELOCITY PREDICTION EQUATIONS .....	69
5.2.1 IMPACT VELOCITY.....	71
5.2.2 IMPACT AIR CONCENTRATION .....	72
<b>CHAPTER 6 .....</b>	<b>73</b>
6.1 CONCLUSIONS .....	73
6.2 RECOMMENDATIONS.....	75
<b>REFERENCES .....</b>	<b>76</b>
<b>APPENDIX A .....</b>	<b>78</b>
<b>APPENDIX B .....</b>	<b>79</b>

## LIST OF TABLES

TABLE 3.1: CALIBRATION COEFFICIENTS FOR BACK-FLUSHING PITOT TUBE.....	28
TABLE 3.2: TESTING MATRIX .....	32
TABLE 4.1: IMPACT DATA .....	37
TABLE 4.2: BACK WALL ZONE VELOCITY COMPONENT DATA .....	49
TABLE 4.3: FLOOR ZONE VELOCITY COMPONENT DATA .....	50
TABLE 4.4: VELOCITY VECTOR DATA .....	51
TABLE 4.5: REGRESSION COEFFICIENTS AND R <sup>2</sup> VALUES .....	61
TABLE 4.6: COMPARISON OF BACK WALL VELOCITIES TO FLOOR VELOCITIES .....	62
TABLE 4.7: COMPARISON OF AVERAGE AND MAXIMUM VECTORS AND COMPONENTS.....	63
TABLE 4.8: MAXIMUM VELOCITIES FOR ALL TESTS .....	64
TABLE 4.9: SPURIOUS CORRELATION.....	66
TABLE 4.10: SEDIMENT TRANSPORT CAPABILITIES, FIELD CONDITION .....	67

## LIST OF FIGURES

FIGURE 2.1: FLOW PATTERNS PRODUCED BY SUBMERGED JET (COLA, 1965) .....	8
FIGURE 2.2: DISTRIBUTION OF PRESSURES ON BOTTOM OF PLUNGE BASIN (LENCASTRE (1961) AS REPORTED BY GEORGE (1980)) .....	10
FIGURE 2.3: AIR PATTERNS FOR VARIOUS RELATIVE LENGTHS OF DUCT (IAMANDI & ROUSE, 1969) .....	12
FIGURE 2.4: REGIONS OF STABLE FLOW FOR A VERTICAL, CIRCULAR BUOYANT JET (LEE & JIRKA, 1981) .....	13
FIGURE 2.5: RADIAL TEMPERATURE TRANSECT (LEE & JIRKA, 1981) .....	14
FIGURE 2.6: STEADY-STATE FLOW FIELDS FOR JET DISCHARGES INTO CONFINED DEPTH. (A) NON-BUOYANT INJECTION. (B) STRONGLY BUOYANT INJECTION. (JIRKA AND HARLEMAN, 1979) .....	16
FIGURE 3.1: PLAN VIEW OF TEST FACILITY .....	18
FIGURE 3.2: ELEVATION OF TEST FACILITY AS VIEWED FROM DOWNSTREAM .....	19
FIGURE 3.3: SIDE ELEVATION OF TEST FACILITY WITH ORIFICE .....	19
FIGURE 3.4: CROSS SECTION OF ORIFICE ASSEMBLY .....	20
FIGURE 3.5: MANIFOLD PIPE HOLE PATTERN (FLATTENED) .....	21
FIGURE 3.6: WEB PLACEMENT IN ORIFICE ASSEMBLY .....	21
FIGURE 3.7: TRAVERSING SYSTEM .....	22
FIGURE 3.8: BACK-FLUSHING PITOT TUBE .....	23
FIGURE 3.9: TRANSDUCER BOARD .....	24
FIGURE 3.10: AIR CONCENTRATION PROBE AND METER .....	26
FIGURE 3.11: CALIBRATION CURVES FOR BACK-FLUSHING PITOT TUBE .....	27
FIGURE 3.12: ACOUSTIC SENSOR .....	29
FIGURE 3.13: COORDINATE SYSTEM .....	31
FIGURE 3.14: VARIABLE DEFINITIONS .....	33
FIGURE 3.15: VELOCITY AT IMPACT COLLECTION LOCATIONS .....	34
FIGURE 3.16: ADV TESTING GRID .....	35
FIGURE 4.1: GENERAL FLOW PATTERNS .....	39
FIGURE 4.2: FLOW PATTERN EXAMPLE .....	39
FIGURE 4.3: CIRCULATION DRIVING FORCES .....	41
FIGURE 4.4: ZONE BOUNDARIES .....	46
FIGURE 4.5: VZ_MIN AT BACK WALL .....	52

FIGURE 4.6: VZ_AVG AT BACK WALL.....	52
FIGURE 4.7: VX_MAX AT FLOOR.....	53
FIGURE 4.8: VX_AVG AT FLOOR.....	53
FIGURE 4.9: VXZ_MAX AT BACK WALL.....	54
FIGURE 4.10: VXZ_AVG AT BACK WALL.....	54
FIGURE 4.11: VXZ_MAX AT FLOOR.....	55
FIGURE 4.12: VXZ_AVG AT FLOOR.....	55
FIGURE 4.13: VZ_MIN AT BACK WALL.....	57
FIGURE 4.14: VZ_AVG AT BACK WALL.....	57
FIGURE 4.15: VX_MAX AT FLOOR.....	58
FIGURE 4.16: VX_AVG AT FLOOR.....	58
FIGURE 4.17: VXZ MAX. AT BACK WALL.....	59
FIGURE 4.18: VXZ AVG. AT BACK WALL.....	59
FIGURE 4.19: VXZ MAX. AT FLOOR.....	60
FIGURE 4.20: VXZ AVG. AT FLOOR.....	60
FIGURE 4.21: VXZ MAX. AND AVG. AT BACK WALL.....	63
FIGURE 4.22: VXZ MAX. AND AVG. AT FLOOR.....	64

## LIST OF SYMBOLS

$a$	= Dimensionless coefficient
$A$	= Adjusted air concentration (air vol./total vol.) in decimal form
$A_u$	= Unadjusted air concentration (air vol./total vol.) in decimal form
$b$	= Dimensionless coefficient
$C_d$	= Drag Coefficient
$d$	= Diameter of sphere with the same volume as a water drop (L)
$g$	= Gravitational acceleration ( $L/T^2$ )
$\Delta h$	= Pressure head differential (L)
$H$	= Drop height measured from issuance to impact (L)
$L$	= Depth in roller region (L)
$L_d$	= Downstream Depth (L)
$m$	= Dimensionless coefficient
$n$	= Dimensionless coefficient
$\Delta p$	= Adjusted pressure head differential (L)
$\Delta p_o$	= Unadjusted pressure head differential (L)
$Q$	= Volumetric discharge ( $L^3/T$ )
$R^2$	= Coefficient of Determination
$V$	= Velocity ( $L/T$ )
$V_i$	= Average impact velocity ( $L/T$ )
$V_o$	= Issuance velocity ( $L/T$ )
$V'$	= Velocity in plunge pool as identified (i.e. $V_{xz\_max}$ ) (cm/s)
Volt	= Voltage (volts)
$V_{x\_avg}$	= Average velocity component in X-direction (cm/s)
$V_{x\_max}$	= Maximum velocity component in X-direction (cm/s)
$V_{xz\_avg}$	= Average velocity vector in XZ-plane (cm/s)
$V_{xz\_max}$	= Maximum velocity vector in XZ-plane (cm/s)
$V_{z\_avg}$	= Average velocity component in Z-direction (cm/s)
$V_{z\_min}$	= Maximum velocity component in the negative Z-direction (cm/s)
$W$	= Ratio of canyon width to jet width
$X_r$	= Distance from upstream boundary to upstream side of jet at impact (L)
$\Pi_1$	= Dimensionless group
$\Pi_2$	= Dimensionless group
$\rho$	= Fluid density ( $M/L^3$ )
$\rho_a$	= Air density ( $M/L^3$ )
$\rho_w$	= Water density ( $M/L^3$ )

## **CHAPTER 1**

### **INTRODUCTION**

When water overtops the crest of a dam, the energy in the flow may erode and/or scour the foundation or abutments on the downstream face of the structure. Many dams are designed to accommodate overtopping and/or utilize spillways with flip buckets or chute blocks to dissipate the energy of the flow. An extreme flood event may force overtopping of a dam which is not designed for such an occurrence. Due to the catastrophic consequences of dam failure, it is important to understand the stability of a dam during an overtopping situation.

The overtopping jet is usually in the form of a highly turbulent, aerated jet and will impact the foundation, dam abutments, and/or the free surface of a plunge pool. When a plunge pool does not exist at the onset of overtopping, a backwater effect will occur at the base of the dam and an artificial plunge pool will usually form. As the jet impacts the water surface and impinges into the plunge pool, the impinging jet induces circulation in the plunge pool. The combination of the impacting jet on the basin floor and circulating flow in the plunge pool can potentially cause sediment degradation from the abutments or basin floor and transport the sediment downstream.

A study was performed focusing on plunge pool circulation and velocity prediction to better understand and enable prediction of flow characteristics in the plunge pool basin between the downstream face of the dam and the jet impact location.

The magnitude of the velocities in the plunge pool upstream of the jet impact area are important because they correspond to the size of sediment that can be dislodged and transported through or out of the plunge pool. The circulation direction results in either sediment aggradation or sediment degradation at the toe of the dam. The study objectives are:

- Determine circulation flow patterns in a plunge pool stilling basin resulting from an impinging jet,
- Determine flow pattern driving forces,
- Determine the effects that changes in impact velocity and impact air concentration have on velocity magnitudes in the plunge pool stilling basin,
- Develop a velocity prediction method for estimating the magnitude and direction of circulation velocities located along the upstream boundary (downstream dam face) and the basin floor in a plunge pool stilling basin.

A literature review was performed focusing on buoyant jets, jet induced flow patterns, and how impacting jets are affected by boundary conditions. A physical model consisting of a free falling, developed, rectangular jet impacting a plunge pool was constructed and operated. A dimensional analysis was performed producing two dimensionless groups. The first group is a function of velocity at impact, air concentration at impact, plunge pool depth, the ratio of basin width to jet width, and gravitational acceleration. The second nondimensional group is a function of the impact velocity and the velocity at the specified location in the basin. Tests were conducted varying discharge, plunge pool tailwater depth, and basin width. Statistical analysis of the results illustrates that the nondimensional groups accurately describe

the velocities in the upstream basin region. A procedure is developed for estimating recirculating velocities in the plunge pool region upstream of the impacting jet and for determining the sediment transport potential from the plunge pool.

## CHAPTER 2

### LITERATURE REVIEW

A review of literature pertaining to jet-induced circulation in a plunge pool was conducted. Most circulation based research has used air as the fluid, while limited research has addressed heavy fluids (i.e., water) in which gravitational effects are significant. When heavy fluids have been examined, most research models have used submerged jets rather than free falling jets which impact a free surface. Research that addresses a greater understanding of flow patterns induced by a free jet impacting a free surface is presented.

#### 2.1 Impact Velocity of a Free Falling Jet

In order to predict the impact velocity of a free falling, undeveloped jet, Ervine and Falvey (1987) proposed using the ballistic equations of motion. The velocity of a free falling, undeveloped jet at impact is described as:

$$V_i = \sqrt{V_o^2 + 2gH} \quad (2.1)$$

where

- $V_i$  = Average impact velocity (L/T)
- $V_o$  = Average initial velocity (L/T)
- $g$  = Gravitational acceleration (L/T<sup>2</sup>)
- $H$  = Drop height (L)

A turbulent, developed jet does not contain a solid core of water which is difficult to analytically describe. Lewis (1996) developed a method for predicting the velocity at impact of a developed jet. By modifying the ballistic equation used by Ervine and Falvey, he was able to account for the air drag which exists in a developed jet. Lewis' equation for the impact velocity of a developed jet is:

$$V_i = \sqrt{V_o^2 + 2gH} - \sqrt{3C_d \left( \frac{\rho_a}{\rho_w} \right) \left( \frac{H}{d} \right) V_o^2} \quad (2.2)$$

where

- $C_d$  = Drag coefficient for sphere (nondimensional)
- $\rho_a$  = Air density (ML/T<sup>2</sup>)
- $\rho_w$  = Water density (ML/T<sup>2</sup>)
- $d$  = Diameter of a sphere with the same volume as a water drop (L)

Lewis' equation assumes that discreet water droplets of uniform diameter exist in the developed jet. Lewis conducted experiments with a developed jet for drop heights of 1.05 m to 1.88 m with issuance velocities of 2.63 m/s to 4.89 m/s.

## 2.2 Jets Confined by Boundaries

As a free falling jet enters into a motionless body of ambient fluid, the shear forces between the two fluids are significant. The shear forces cause the motionless fluid to be entrained with the fluid jet, thus creating motion in the once motionless fluid. When equilibrium exists between the fluid jet and the surrounding body of fluid, flow patterns will develop. Under certain boundary conditions, the jet may be dispersed and become entrained in the surrounding flow in such a way that portions of the dispersed jet re-enter the fluid jet. This process is defined as circulation. Circulation can cause

fluid at significant distances from the jet to be entrained into motion. When boundary effects are not present, the jet will diffuse in the longitudinal and lateral directions such that entrainment of the ambient fluid occurs, but circulation may not.

Many researchers have investigated the effects of a boundary in the longitudinal direction using both circular and rectangular jets. Most research examining boundary effects has used a free jet impacting a surface without a water cushion or lateral boundaries. A water cushion is a body of water which is between the issuance location of a jet and the longitudinal boundary. For models without a water cushion, researchers have investigated the velocities in the jet prior to impact, velocities of the deflected jet along the surface (wall jet), and the pressures on the surface at the point of impact (Beltaos and Rajaratnam, 1973; Beltaos, 1976; and George, 1980).

When a water cushion and an immobile longitudinal boundary (i.e., plywood, concrete, etc.) were considered, most research has focused on the pressure distribution at the floor of the basin. Ervine and Falvey (1987) stated that the pressures experienced in the plunge pool basin are a function of the following: the jet's ability to spread laterally, the ability of the jet to become increasingly distorted during the plunge into the basin, and the ability of the jet to break up and dissipate if the plunge pool is sufficiently long. They also found that developed aerated jets produce smaller mean pressures than jets with low air content. For models using a water cushion, the point of jet issuance was typically placed below the free surface. Submergence of the water jet's issuance location was required because the air entrainment which occurred when a free jet impacted a free surface caused measuring devices to be inaccurate or inoperable.

Extensive research has also been conducted concerning the amount of sediment which is removed from a movable sediment floor due to the forces of a submerged jet. Breusers (1991) conducted an experiment focusing on scour using a submerged jet with and without air entrainment. He reported that when the issuance velocities of the aerated and non-aerated submerged jets were equal, the volume of boundary material scoured by a jet with 50 percent entrained air was less than that scoured by a submerged jet without air entrainment. This reinforced the findings of Ervine and Falvey that the velocity of a jet entering a water cushion or plunge pool with a significant concentration of air will decay faster than that of a solid water jet, resulting in a reduced potential for erosion. Bohrer (1996) confirmed that the velocity of a jet will decay more quickly when air is entrained. Bohrer also developed a method to estimate the velocity of a developed jet in the jet impact region at any distance below the water's surface.

Albertson, Dai, Jensen, & Rouse (1950) conducted an experiment using air and a rectangular shaped duct. It was found that at large distances from the jet, the velocities in the duct dissipate to a point at which the flow patterns are driven by extraneous effects rather than those of the jet. This lead to the need for experiments concerning the effects of varying boundary conditions. The following section discusses a few experiments which provide insight into the flow patterns which may be expected as a result of a plunging jet with boundary effects.

## 2.3 Flow Patterns and Circulation

### 2.3.1 Cola

Cola (1965) studied the effects of a boundary on the diffusion of a rectangular water jet impacting the free surface of a plunge pool. Secondary benefits of the research were a general mapping of the flow patterns in the basin. The model consisted of the jet entering a symmetrical rectangular basin with 0.8 meter high weirs at 3.9 meters from jet centerline at each end. The jet width and basin width were approximately equal. Cola found that a great amount of air that was drawn into the basin by the jet impacting the free surface. He stated that at certain depths, the buoyancy force due to the bubbles prevailed over the drawing force of the jet. Because of buoyancy forces and instrumentation problems, the outlet of the jet was lowered so that the jet issuance was submerged, eliminating air entrainment. The flow patterns produced in the model by Cola were symmetric on each side of the jet. Only general flow patterns were mapped as presented in Figure 2.1.

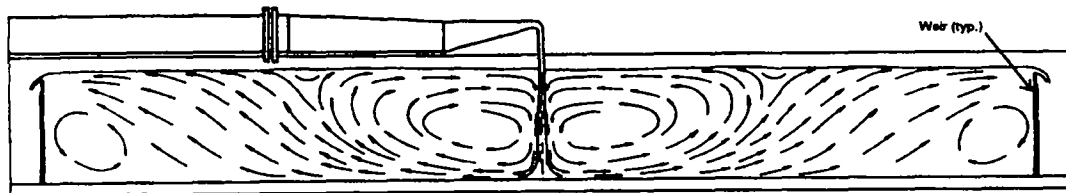


**Figure 2.1: Flow Patterns Produced by Submerged Jet (Cola, 1965)**

Cola found that as the issuance velocity increased, the location of the upward flow on each side moved closer to the weirs. He also discovered that negative pressures were present along the floor near the impact region. The negative pressures were

determined to be the product of both a rebound effect of the jet bouncing off the floor's surface and the resulting upward flows.

### 2.3.2 Lencastre

Lencastre, as reported by George (1980), experimented with a vertical, rectangular water jet issuing downward into a rectangular basin with an upstream boundary. The point of issuance was not submerged, allowing air to be entrained into the jet as it impacted the water surface. He determined that the flow had a rebound effect off of the floor, causing upward flows and negative pressures along the floor as presented in Figure 2.2. As depicted,  $H$  is pressure,  $H_c$  is the pressure without a water cushion,  $c$  is the tailwater depth,  $b$  is the slot thickness, and  $y$  is the axis in the longitudinal direction. Lencastre's results indicated that pressures at the floor were lower than those documented by Cola. The air entrainment in Lencastre's tests, which was eliminated in Cola's tests, caused the velocities in the pool to decay more quickly, resulting in lower pressures at the floor. Due to the upstream boundary in Lencastre's experiment, cross-flow was present increasing the complexity of the flow patterns. Cross-flow is fluid traveling in the downstream direction which crosses the path of the jet. Lencastre was unable to determine the effect the cross-flow had on the rebound effect. Flow patterns were not reported.

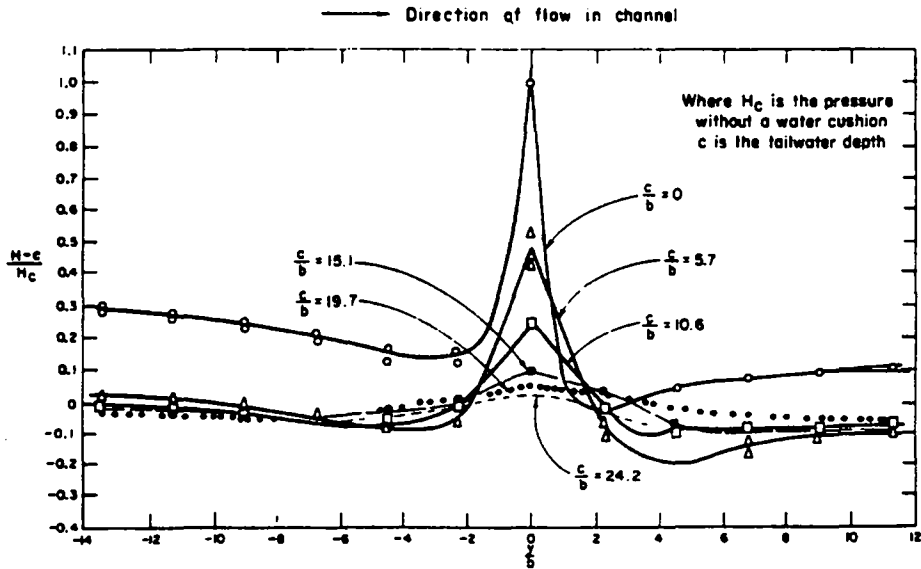


**Figure 2.2: Distribution of Pressures on Bottom of Plunge Basin (Lencastre (1961) as reported by George (1980))**

### 2.3.3 lamandi and Rouse

lamandi and Rouse (1969) investigated a submerged, rectangular jet issuing upwards into a basin. The model was designed to represent submerged jets or bubble screens whose purpose is to create circulation. The original intent was to use water as the model fluid, but difficulty in creating accurate measuring devices forced the use of air. Air was blown into a duct through a variable width slot in the floor at one end of the duct. The jet angle is upward and is located at  $x/D=0$ , as presented in Figure 2.3; the rectangular outlet is at approximately  $x/D=0.5$ . As depicted in Figure 2.3,  $x$  is the longitudinal axis,  $y$  is the vertical axis,  $D$  is the duct height (height and width are equal),  $m$  is the momentum flux, and  $\rho$  is the fluid density. The duct measured two feet square with a movable downstream wall, allowing a maximum distance of eight feet from the point of issuance. A hot-wire anemometer was used for velocity magnitude

measurement. Threads and paper streamers were used to determine locations of abrupt flow direction change. The flow patterns were derived by plotting lines through data points of equal value creating lines of constant velocity.

Iamandi and Rouse found that when the vertical and horizontal dimensions of the fluid body are similar, a single vortex is produced. However, once the length exceeds some multiple of the depth, a second, weaker vortex rotating in the opposite direction as the first will be formed. A series of vortices may result if the fluid body is sufficiently long, yet eventually the dissipated velocities are too low to create distinct flow patterns. Iamandi and Rouse also stated that their model would be indicative of both air and water at any angle of issuance. This statement is true for air, however, it may not apply when a heavy fluid and air are mixed. When an aerated heavy fluid is used, gravitational effects and issuance orientation become important because the direction of the jet and that of the buoyancy force will not always be the same. The flow patterns observed are documented in Figure 2.3.

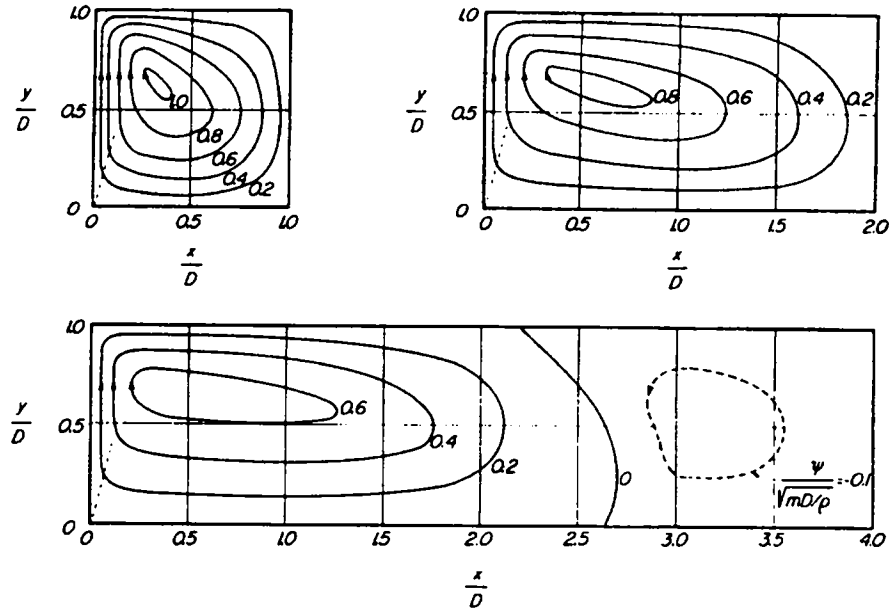


**Figure 2.3: Air Patterns for Various Relative Lengths of Duct (Iamandi & Rouse, 1969)**

#### 2.3.4 Lee and Jirka

Lee and Jirka (1981) conducted experiments with a circular, upward facing buoyant jet to determine when stability did and did not occur. The term stable refers to a no circulation condition, while unstable refers to the occurrence of circulation. The buoyancy of the jet in the experiment was attributed to a temperature differential between the jet and the fluid in the basin. The location of jet issuance was at the floor of a basin at mid-length of a model with large horizontal extent. The depth of the pool was varied, resulting in varied circulation patterns. Four regions of flow were defined for the stable condition: (I) Initial Buoyant Jet Region (II) Surface Impingement Region (III) Radial Internal Hydraulic Jump Region, and (IV) Stratified Counter Flow Region. The four regions of stable flow are shown schematically in Figure 2.4.

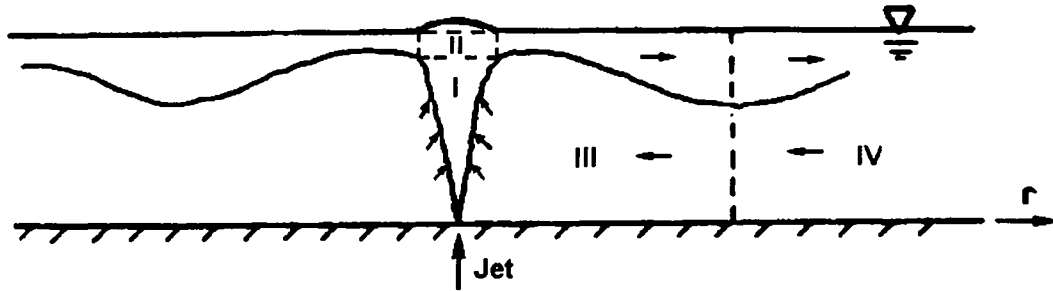


**Figure 2.4: Regions of Stable Flow for a Vertical, Circular Buoyant Jet (Lee & Jirka, 1981)**

For the unstable flow condition, distinct flow regions were not defined. It was concluded that a surface hump (boil) is created when the buoyant jet impinges on the free surface (Region II). This in turn gives rise to a radial pressure gradient (for a circular jet) and horizontal spreading of the mixed discharge (above Regions III and IV). Temperature measurements were made in order to determine the amount of mixing and circulation; velocity was not measured. In order to determine the stability (stable or unstable) of the system, a densimetric Froude number and the submergence (ratio of water depth to jet diameter) were used:

$$F_o = \frac{u_o}{\sqrt{g \frac{\Delta\rho_o}{\rho_a} D}} \quad (2.3)$$

where

- $F_o$  = Densimetric Froude number
- $u_o$  = Injection velocity
- $g$  = Gravitational acceleration
- $\Delta\rho_o/\rho_a$  = Relative density difference between heated water and the ambient fluid
- $D$  = Jet diameter

Stability was dependent on the buoyancy of the jet. Lee and Jirka were able to predict the stability of the model system using the densimetric Froude number and

submergence. One flow pattern reported illustrates the rebound effect of the jet after impact upwards with a free surface (Figure 2.5).

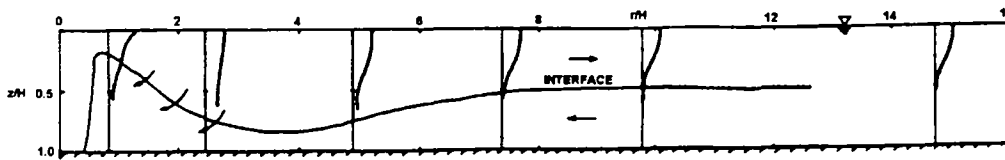


**Figure 2.5: Radial Temperature Transect (Lee & Jirka, 1981)**

The rebound effect attributed to the free surface caused the buoyant flow to deflect well below one half the depth of the fluid. The force of the rebound is great enough to drive the less dense fluid down into the lower, more dense layer. The upper boundary, in this case the free surface, is flexible (non-rigid) and diffused the upward velocities via the surface boil more than would a rigid boundary.

### 2.3.5 Jirka and Harleman

Jirka and Harleman (1979) performed a study similar to Lee and Jirka to predict the stability of flow patterns caused by a buoyant jet, however a rectangular jet was used instead of a circular jet and the basin was of finite length. The location of jet issuance, type of jet, and all other model characteristics were as reported by Lee and Jirka. In order to determine the stability (stable or unstable) of the system, the densimetric Froude number and the submergence (ratio of water depth to slot width) were used:

$$F_o = \frac{u_o}{\sqrt{g \frac{\Delta\rho_o}{\rho_a} B}} \quad (2.4)$$

where

- $F_o$  = Densimetric Froude number
- $u_o$  = Injection velocity
- $g$  = Gravitational acceleration
- $\Delta\rho_o/\rho_a$  = Relative density difference between heated water and the ambient fluid
- $B$  = Slot width

Jirka and Harleman confirmed lamandi and Rouse's findings concerning the formation of multiple vortices. They found that only one vortex was formed up to two and one half times the depth away from the jet. Outside this distance, a second, weaker vortex formed. It was also noted that longitudinal boundaries will fix the location of a vortex. However, for highly buoyant jets, vortices did not form and circulation did not occur due to the creation of an interface which acted as a boundary between the buoyant flow and the existing fluid in the basin. The formation of vortices and an interface are presented in Figure 2.6. Velocity measurements were attempted by using photographs of dye traces, yet the results were not conclusive nor discussed.

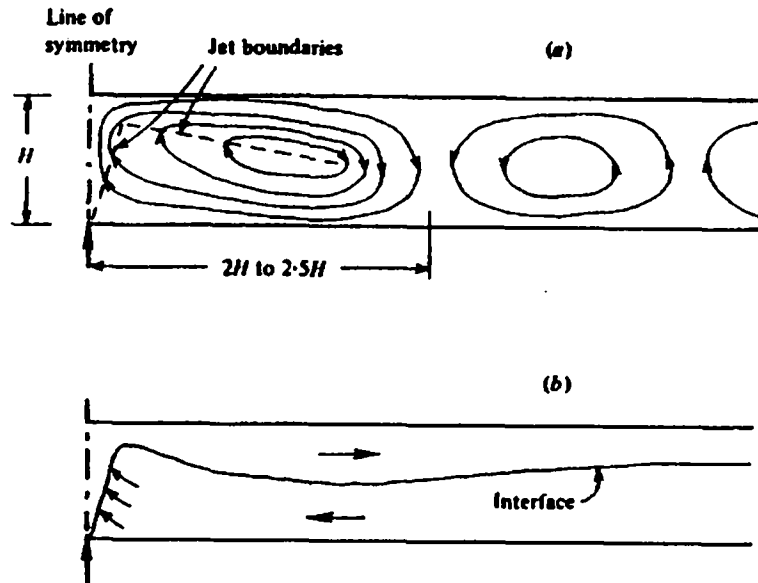


**Figure 2.6: Steady-state flow fields for jet discharges into confined depth. (a) Non-buoyant injection. (b) Strongly buoyant injection. (Jirka and Harleman, 1979)**

These experiments provided insight into the actions of jets influenced by boundary conditions. Velocity dissipation, the rebound effect, circulation (stability), and general flow patterns were discussed. Major influences on the flow patterns were determined to be angle of jet issuance, buoyancy of the jet, and geometry. A densimetric Froude number was determined to be an important parameter in describing the stability of flow patterns.

## **CHAPTER 3**

### **TEST PARAMETERS**

The flow patterns and velocities in a plunge pool upstream of the jet impact location resulting from an impacting free falling jet were examined under a variety of test conditions. The test facility, model description, instrumentation and testing conditions are presented.

#### **3.1 Location of Test Facility**

The test facility is located in the Hydraulics Laboratory at the Engineering Research Center at Colorado State University, Fort Collins, Colorado. Water was derived from Horsetooth Reservoir located one-half mile west of the laboratory.

#### **3.2 Model Description**

The test facility is a physical model consisting of a sump, pump, pipe network with delivery pipe with orifice assembly, test basin, viewing platform, stop logs for tailwater control, outflow sediment trap, and a wasteway to channel flow back to the sump as illustrated in Figure 3.1 through Figure 3.3. All tests were performed with clear water. The basin dimensions are 4.23 m long, 1.52 m high, and variable width with a maximum of 3.05 m. Vertical walls were aligned in the downstream direction to decrease the lateral width of the basin. Water is pumped from the sump through the pipe network using a 40-horsepower pump. The pipe connects to an orifice assembly that is designed to create a highly turbulent condition which simulates a free falling jet

that occurs when a dam overtops. The circulation pattern (vortex) formed in the basin on the upstream side of the impacting jet is defined as the roller.

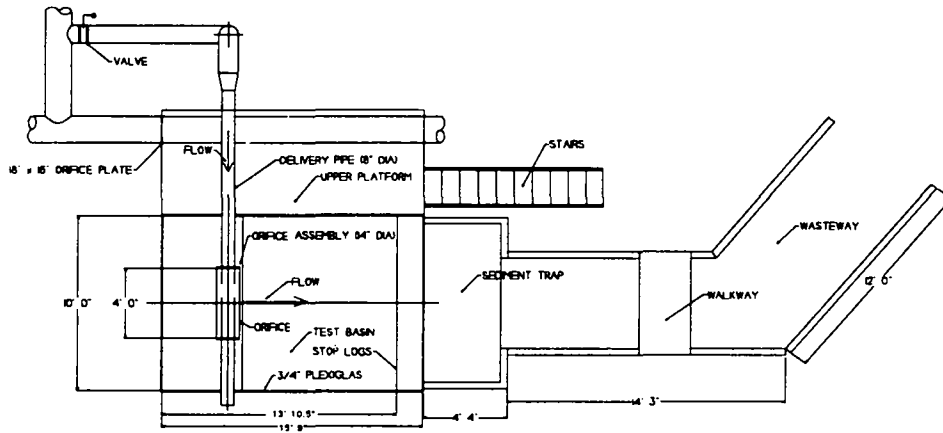


**Figure 3.1: Plan View of Test Facility**

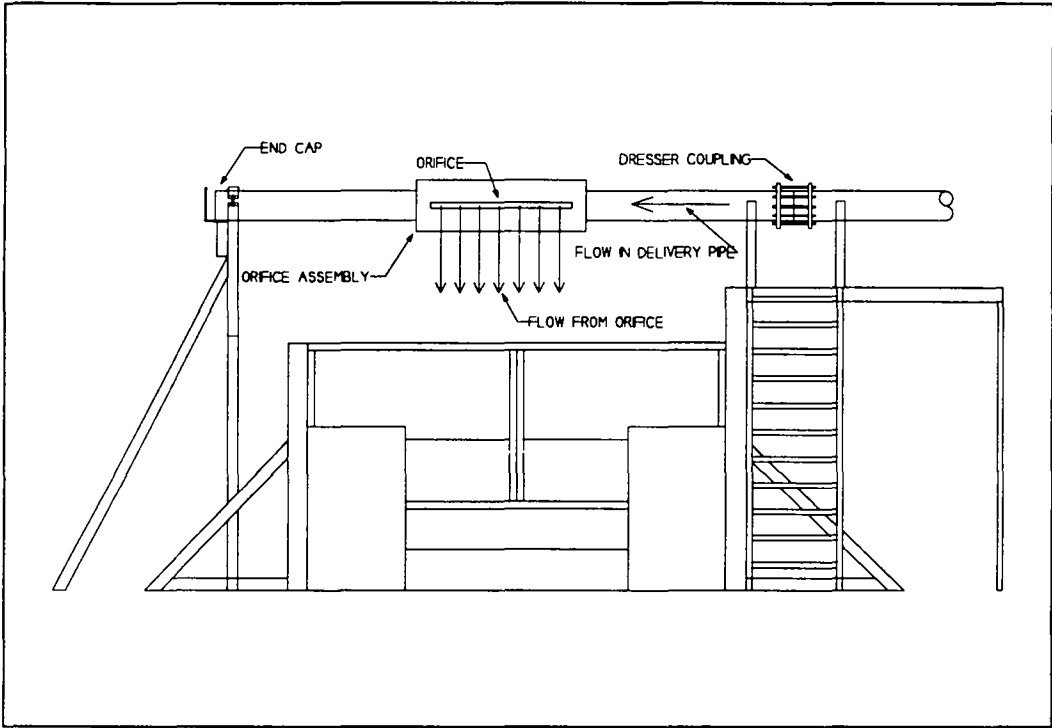


**Figure 3.2: Elevation of Test Facility as Viewed from Downstream**

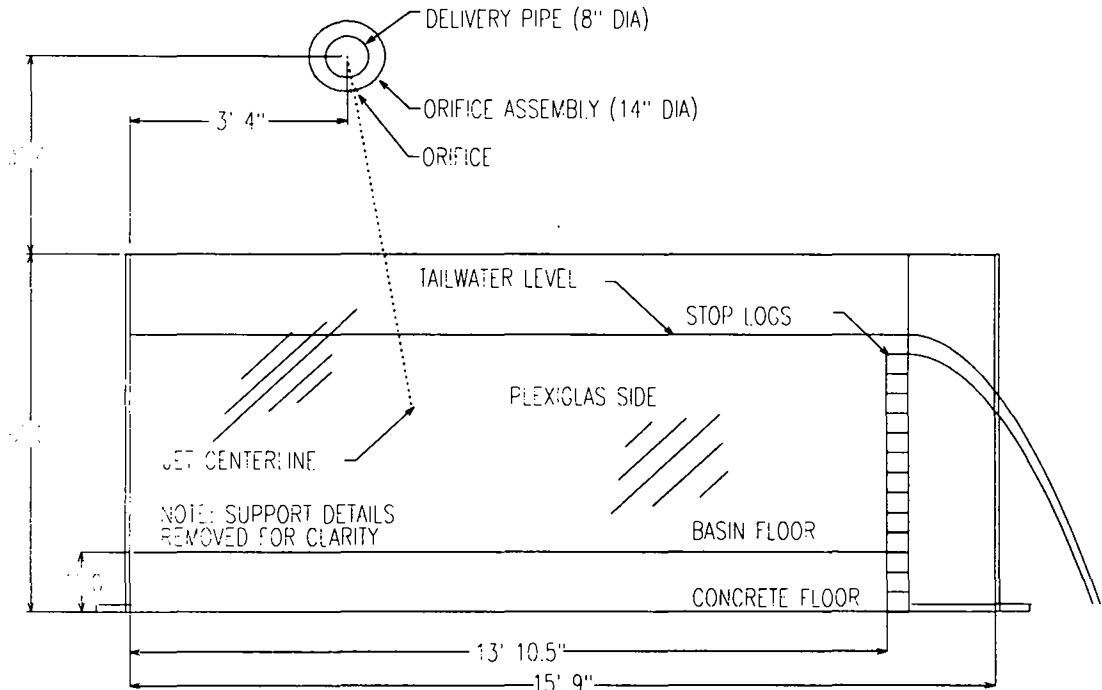


**Figure 3.3: Side elevation of Test Facility with Orifice**

The orifice assembly consists of the delivery pipe and an outer, concentric shell with outlet vanes as shown in Figure 3.4. In order to create the desired jet condition at issuance, the manifold hole pattern is as presented in Figure 3.5. Flow passes through the manifold, around the inside of the shell, and emits from the outlet vanes through the nozzle into the atmosphere. Also included in the assembly are concentric webs which increase the uniformity of the jet as presented in Figure 3.6. The orifice assembly emits a rectangular, developed jet that free falls and impacts the water surface in the test basin. The jet impinges into the basin, flows over the stop logs, through the sediment trap, and through the wasteway.

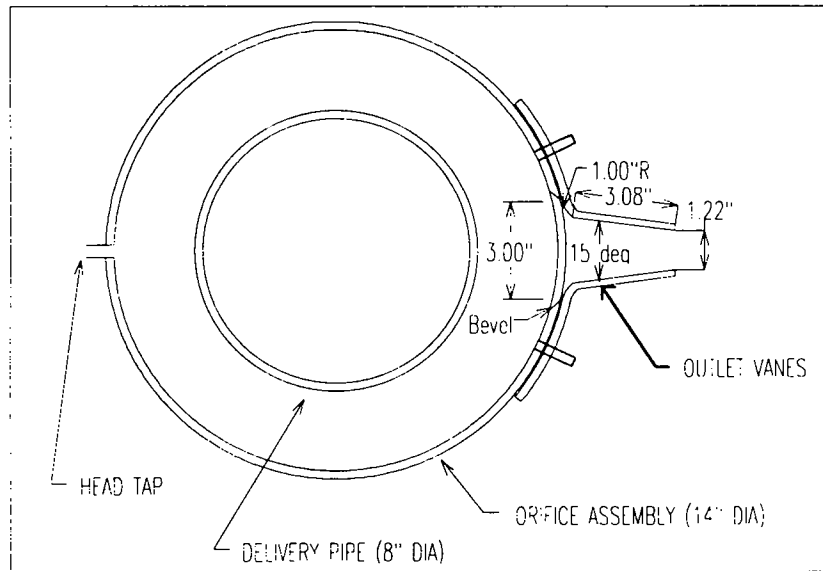


**Figure 3.4: Cross Section of Orifice Assembly**

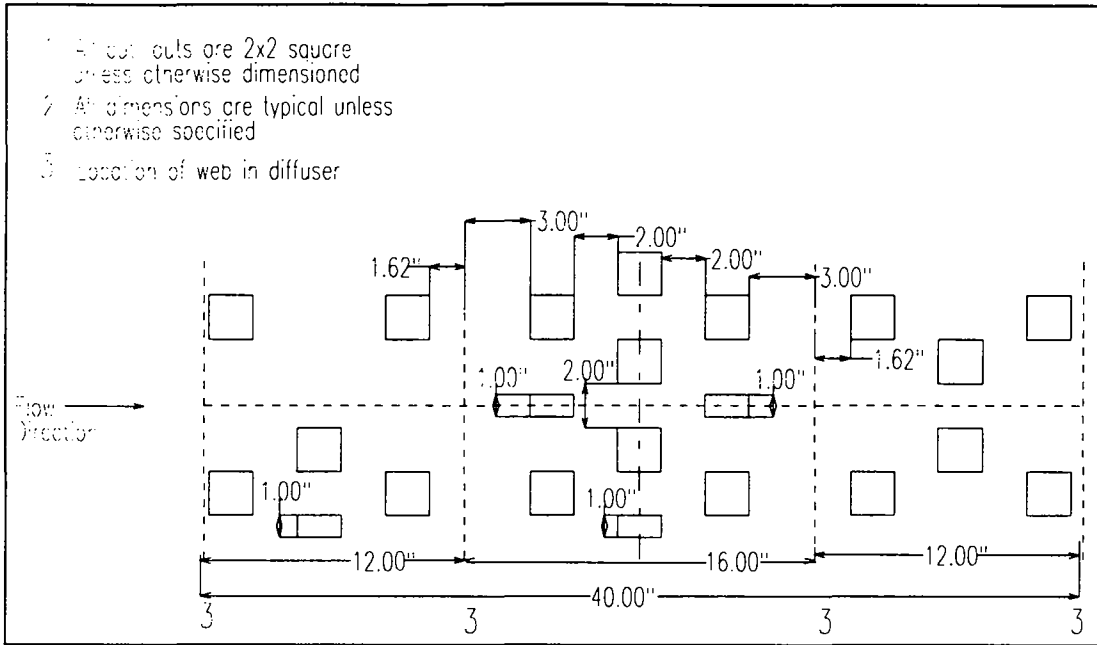


**Figure 3.5: Manifold Pipe Hole Pattern (flattened)**

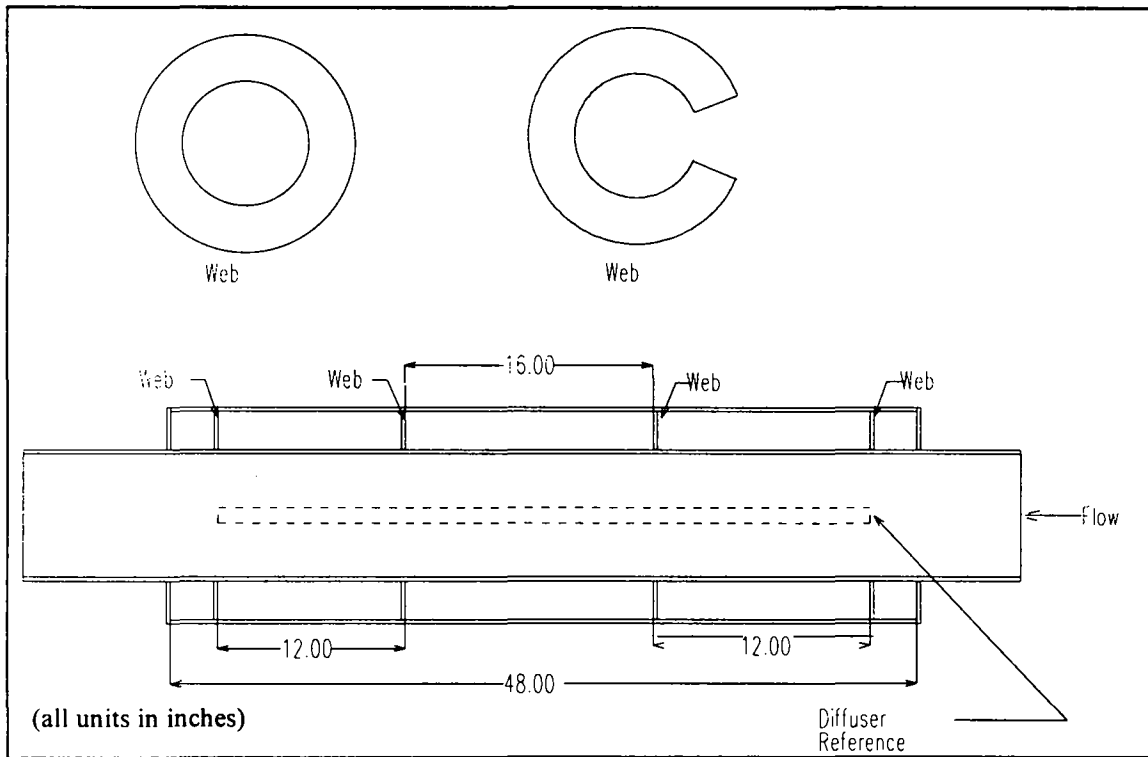


**Figure 3.6: Web placement in Orifice Assembly**

### 3.3 Instrumentation

The discharge, velocity at impact, air concentration at impact, and flow patterns and velocities in the test basin are measured using a spectrum of instrumentation. A vertical gage system and a horizontal traversing system were mounted on rails on top of the basin walls allowing the positioning of the instrumentation at any location inside the basin as schematically shown in Figure 3.7.

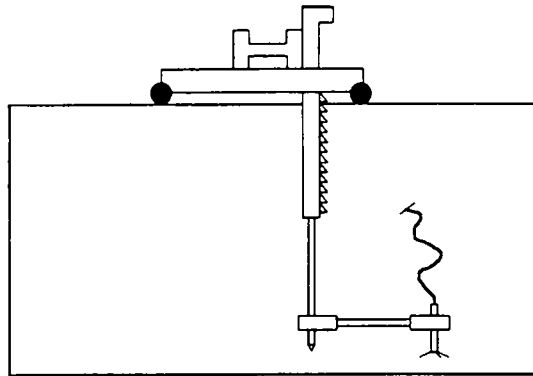


**Figure 3.7: Traversing System**

#### 3.3.1 Orifice Plate

The pipe network contains a calibrated orifice plate which is used to measure the discharge entering the model. The calibration equation is:

$$Q = 8.3552\sqrt{\Delta h} \quad (3.1)$$

where

$Q$  = volumetric discharge (ft<sup>3</sup>/s)  
 $\Delta h$  = pressure head differential (ft)

The pressure head differential is measured using a manometer board accurate to 0.002 ft. The accuracy of the orifice plate is  $\pm 2\%$ .

### 3.3.2 Back-Flushing Pitot Tube

In order to measure the velocity of a developed jet at a specific point, the velocity and the air concentration must be measured. A back-flushing pitot tube developed by the U.S. Bureau of Reclamation is used to measure velocity as pictured in Figure 3.8 (Frizell, Ehler, and Mefford, 1994). A back-flushing pitot tube is used rather than a conventional pitot tube to eliminate the introduction of air into the pitot lines. The back-flushing pitot tube is attached to a variable angle mount which is connected to the vertical point gage system enabling the tip of the probe to be set parallel to the direction of flow.

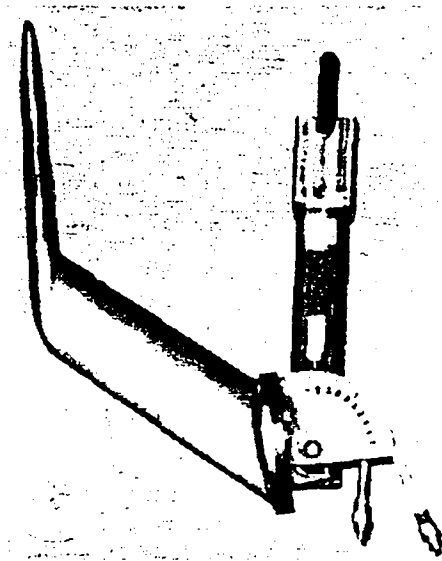


**Figure 3.8: Back-Flushing Pitot Tube**

The back-flushing pitot tube emits water from both static and dynamic ports. Rotameters and a pressure regulator are used to maintain a constant discharge of 3 gallons per hour through each port. A transducer board (Figure 3.9) is employed to regulate the back-flushing discharges and receive the static and dynamic pressures from the back-flushing pitot tube. The pressure differential between the static and

dynamic ports is received by a Stathium® PM300 differential pressure transducer and converted to a voltage. The output voltage is channeled through a Hewlett Packard 8875 Differential Amplifier and then to a DAS-1600 data collection board which is located in a 386-25 MHz computer. Keithley ViewDac® software is used to record a time-averaged voltage for each data collection point. The unadjusted pressure differential corresponding to voltage is calculated via the calibration equation:

$$\Delta p_o = 5.322 * \text{Volt} - 1.2457 \quad (3.2)$$

where

- $\Delta p_o$  = Unadjusted pressure head differential (L)
- Volt = Voltage (volts)

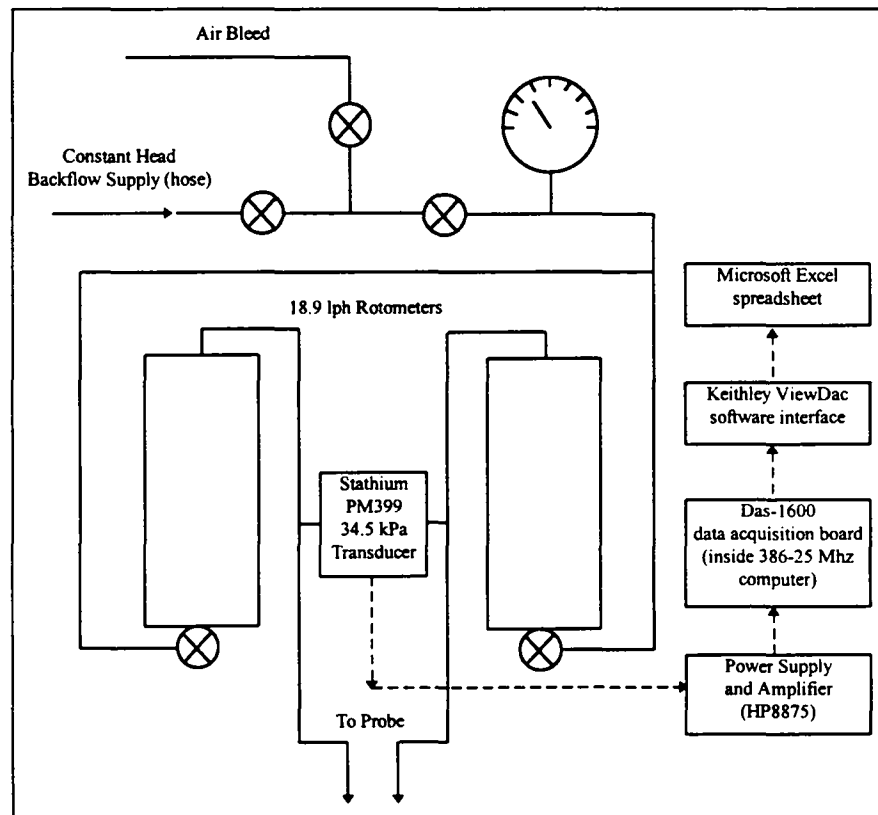


**Figure 3.9: Transducer Board**

The adjusted pressure head differential ( $\Delta p$ ) is calculated by subtracting the baseline pressure head differential measured in quiescent water from the unadjusted pressure head differential at each location. The following equation transforms the adjusted pressure head differential into velocity:

$$V = \sqrt{\frac{2\Delta p}{\rho}} \quad (3.3)$$

where

- $V$  = Velocity (L/T)
- $\Delta p$  = Adjusted pressure head differential (L)
- $\rho$  = Fluid density (M/L<sup>3</sup>)

It is evident from Equation 3.3 that the velocity is dependent on the density of the fluid. Therefore, an air concentration probe is used in combination with the back-flushing pitot tube to accurately measure the velocity of the developed jet.

### 3.3.3 Air Concentration Probe

The density of a jet changes as it translates through air, impacts a free surface, and penetrates into a basin. Thus, a single velocity measurement requires that the placement of the back-flushing pitot tube and the air concentration probe be in the same position. The air concentration probe illustrated in Figure 3.10 was developed by the U.S. Bureau of Reclamation (Frizell et al., 1994). The probe tip consists of two platinum wires which act as an electrical resistively sensor in water. When air bubbles greater than 0.2 mm in diameter pass between the wires, the resistivity increases. The higher the resistivity, the lower the voltage across the probe. The air concentration probe is connected to a meter which converts the voltage into an unadjusted percent air

volume per total volume ( $A_u$ ) and is digitally displayed. Initialization of the probe prior to each test requires two steps. First, balancing the anti-plating signal prevents the tip of the probe from obtaining a charge. Second, adjusting the air meter gain accounts for the conductivity of the water. Adjusted air concentration ( $A$ ) is calculated using the calibration equation:

$$A = -0.5157A_u^2 + 1.3461A_u + 0.09556 \quad (R^2 = 0.991) \quad (3.4)$$

where

$A$  = Adjusted air concentration (decimal)

$A_u$  = Unadjusted air concentration (decimal)

The air concentration probe is attached to a variable angle mount allowing the tip of the probe to be aligned parallel to the impacting jet.

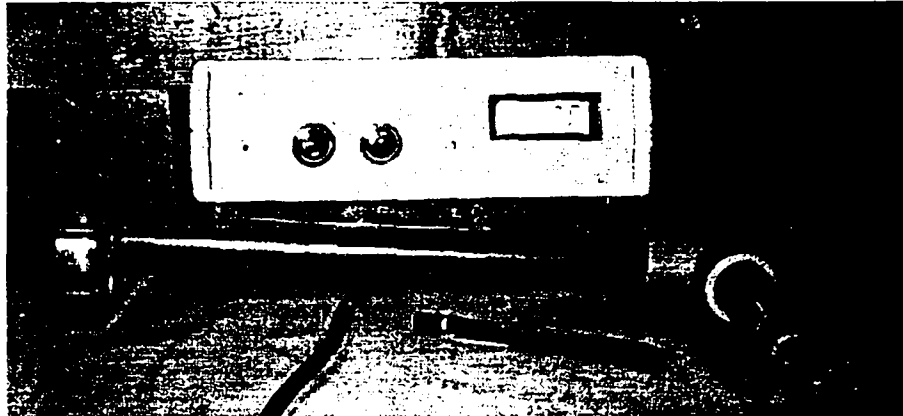


**Figure 3.10: Air Concentration Probe and Meter**

The back-flushing pitot tube was calibrated producing four curves based on 0, 40, 60, and 80 percent air concentrations as presented in Figure 3.11. The calibration equation for the back-flushing pitot tube is of the form:

$$V = a\Delta p^b \quad (3.5)$$

where

- $V$  = Flow velocity (L/T)
- $\Delta p$  = Adjusted pressure head differential (L)
- $a$  = Dimensionless coefficient
- $b$  = Dimensionless coefficient

Table 3.1: presents the coefficients for the four curves in Figure 3.11. For each location at which data are obtained, a set of back-flushing pitot tube calibration curves based on air concentration are interpolated to calculate the corresponding velocity. For example, if the air concentration at a given location is 50%, the velocity values on the 40% and 60% air concentration curves for the given adjusted pressure head differential are used for calculating the interpolated velocity value.

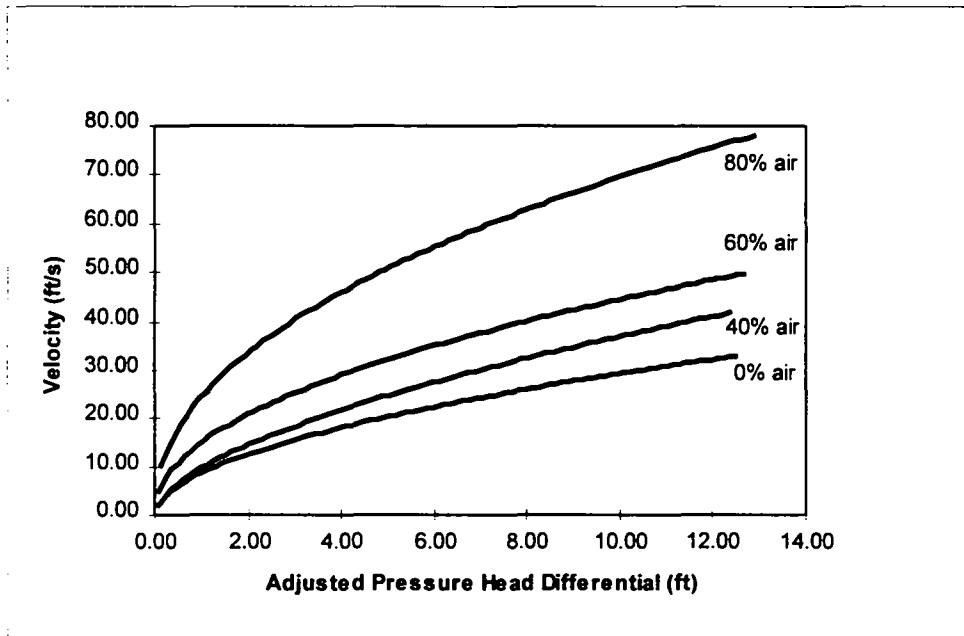


**Figure 3.11: Calibration Curves for Back-Flushing Pitot Tube**

**Table 3.1: Calibration Coefficients for Back-Flushing Pitot Tube**

Percent Air	Coefficient, <i>a</i>	Coefficient, <i>b</i>
0	8.76	0.5239
40	9.71	0.5801
60	15.05	0.4708
80	24.49	0.4537

Combining the back-flushing pitot tube and the air concentration probe produce an error range of  $\pm 8\%$  (Frizell et al., 1994).

#### 3.3.4 Acoustic Doppler Velocimeter

A SonTek® three-dimensional Acoustic Doppler Velocimeter (ADV) is used to map the flow patterns and measure the velocities in the roller region of the plunge pool. The roller region is defined as the region of the basin between the upstream side of the jet and the upstream boundary of the basin.

The ADV consists of an acoustic sensor, a signal conditioning module, and a signal processing board which is used in coordination with a data acquisition board in a 386-25 MHz computer. The acoustic sensor consists of an acoustic transmitter and three acoustic receivers as illustrated in Figure 3.12. The acoustic transmitter emits a signal which is reflected off of suspended sediment particles, air bubbles, etc. The shift in the signal received by the three acoustic receivers allows the ADV to calculate the velocity of the particle in three orthogonal directions. SonTek® software is used in coordination with the ADV to set the sampling rate, water temperature and salinity, and recording options. Water temperature and salinity are required for the Doppler calculations within the software.

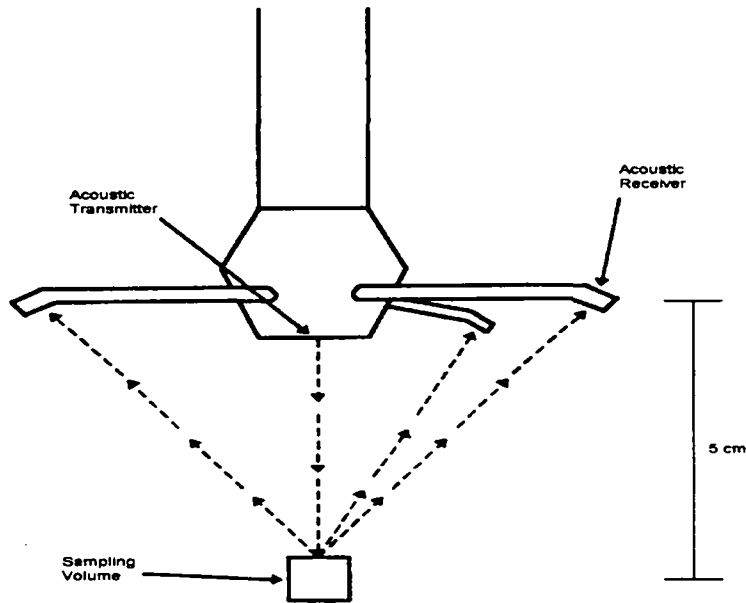


**Figure 3.12: Acoustic Sensor**

The sampling rate and recording period used by the ADV data collection software are variable: the sampling rate ranges from 0.1 Hz to 25 Hz and the maximum recording period is limited by the computer's storage capacity. Due to turbulence and surging in the roller region, an optimal sampling rate and optimal recording period were determined such that accurate time-averaged data were acquired in the shortest period of time. The effects of turbulence and surging were minimized by using a sampling rate of 25 Hz for a recording period of 90 seconds per location. Lohrmann, Cabrera, and Kraus (1994) stated that point velocity measurements taken with the ADV are accurate to  $\pm 2\%$ .

### 3.3.5 Marsh-McBirney® Velocity Meter

A Marsh-McBirney® one-dimensional velocity meter was used to confirm velocity magnitude and flow direction data acquired by the ADV. The Marsh-McBirney® velocity meter measures changes in the magnetic field around the probe to determine the magnitude of the velocity with an accuracy of  $\pm 2\%$  (Marsh-McBirney®, Inc., 1985). The direction of the flow was determined by manually rotating the probe until the direction of maximum velocity was located.

### 3.4 Coordinate System

A coordinate system was established as shown in Figure 3.13. The origin is located on the basin floor at the upstream corner. The positive X-direction is downstream, the positive Y-direction is in the lateral direction, and the positive Z-direction is vertically upward.

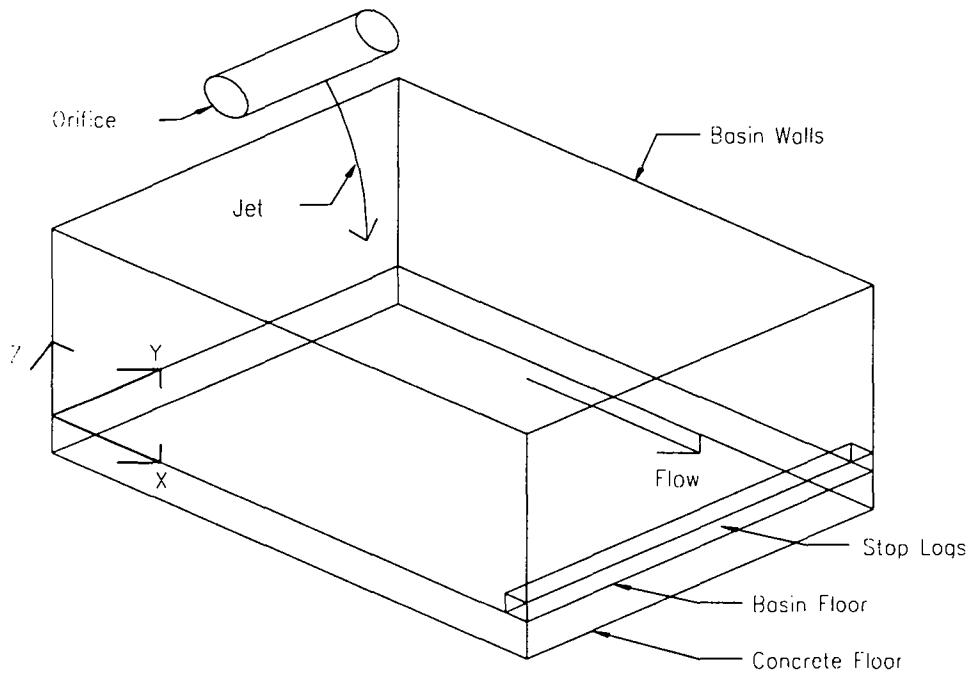


**Figure 3.13: Coordinate System**

### 3.5 Testing Matrix

The test variables are discharge ( $Q$ ), tailwater depth at a location downstream where normal depth exists ( $L_d$ ), and the ratio of the basin (canyon) width to the jet width ( $W$ ). Nine tests were conducted using three, four, and five cubic feet per second (cfs) at three tailwater depths. For each of these tests, three basin widths were investigated. The lateral basin width ratio,  $W$ , equals the canyon width divided by the jet width. The  $W$  ratios investigated were 1:2, 1:1, and 3:1. The lateral width ratios were adjusted by inserting vertical walls into the basin aligned in the downstream direction. The angle of jet issuance was constant at 18 degrees from vertical for all experiments. The tests are summarized in Table 3.2.

**Table 3.2: Testing Matrix**

Test No.	Discharge, Q (cfs)	Stop Log Height (ft)	Width Ratio, W
01	3	1.35	3:1
02	3	2.50	3:1
03	3	3.39	3:1
04	5	1.35	3:1
05	5	2.50	3:1
06	5	3.39	3:1
07	3	1.35	1:1
08	3	2.50	1:1
09	3	3.39	1:1
10	5	1.35	1:1
11	5	2.50	1:1
12	5	3.39	1:1
13	4	1.35	1:1
14	4	2.50	1:1
15	4	3.39	1:1
16	4	1.35	3:1
17	4	2.50	3:1
18	4	3.39	3:1
19	3	1.35	2:1
20	3	2.50	2:1
21	3	3.39	2:1
22	4	1.35	2:1
23	4	2.50	2:1
24	4	3.39	2:1
25	5	1.35	2:1
26	5	2.50	2:1
27	5	3.39	2:1

### 3.6 Testing Procedures

During each test, data were collected pertaining to the discharge, jet, and plunge pool basin. The procedures used to obtain these data are described herein.

Tailwater depths are measured in the roller region ( $L$ ) and at a location downstream of jet impact where the flow approaches normal depth ( $L_d$ ) as presented in Figure 3.14. Also shown in Figure 3.14 is the distance between the upstream boundary and the upstream side of the jet at impact,  $X_r$ . The jet width, breadth, impact angle, and impact location are also measured at the impact plane. The impact plane is defined as the water surface elevation where normal depth exists. The tailwater depths and jet

dimensions are entered into Excel®, resulting in data collection coordinates for the back-flushing pitot tube, air concentration probe, and ADV.

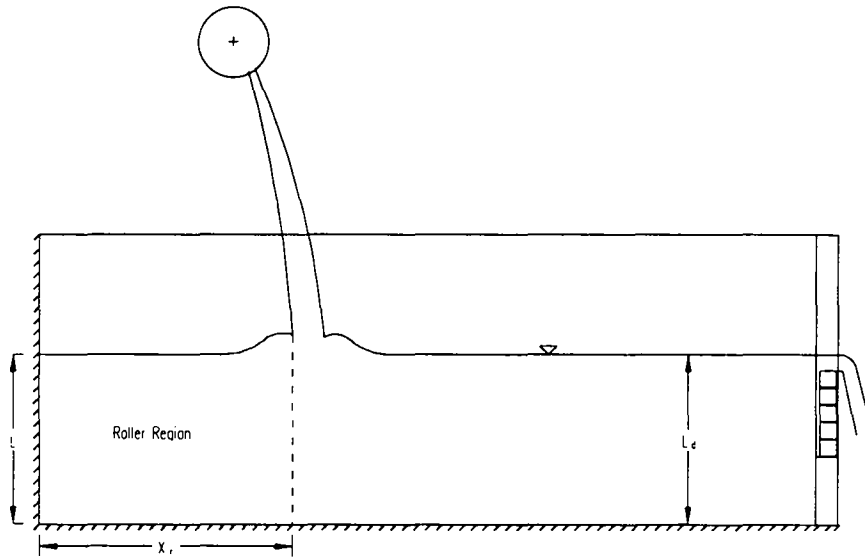


**Figure 3.14: Variable Definitions**

Impact velocity ( $V_i$ ) is determined using both the back-flushing pitot tube and the air concentration probe. Impact velocity data are collected at the impact plane with both probes at five points along the width of the jet at the breadth centerline, as illustrated in Figure 3.15. For each of the five data collection locations, the time-averaged velocity is calculated using Equation 3.5. The average of the five time-averaged velocity points results in a single time-averaged impact velocity ( $V_i$ ) for each test.

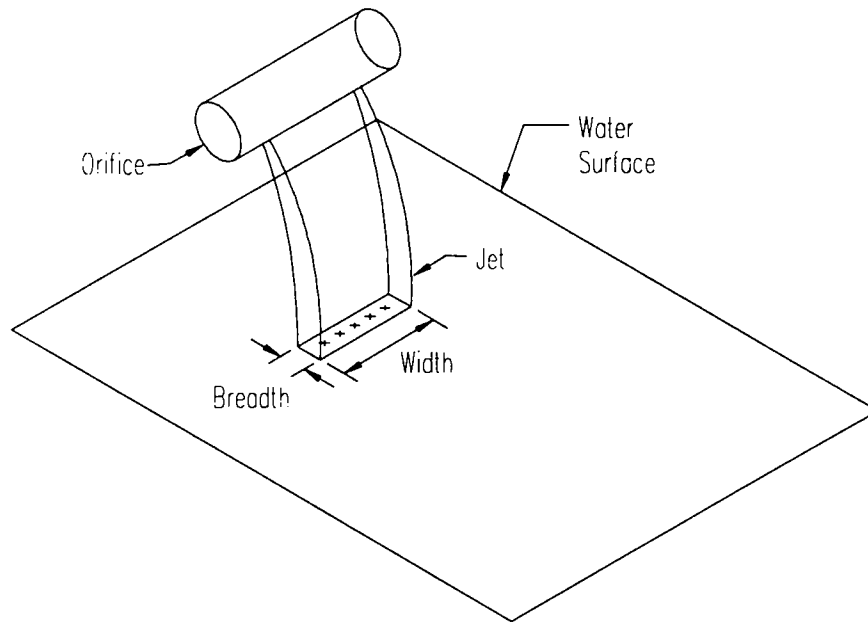


**Figure 3.15: Velocity at Impact Collection Locations**

ADV data are acquired at the intersections of three orthogonal planes in the roller region. Locations of the outermost planes are selected such that the velocities along the upstream wall and the floor are obtained. Intermediate planes for ADV data collection are chosen such that the flow patterns and corresponding velocities throughout the roller region are attained. Figure 3.16 illustrates a typical ADV testing grid.

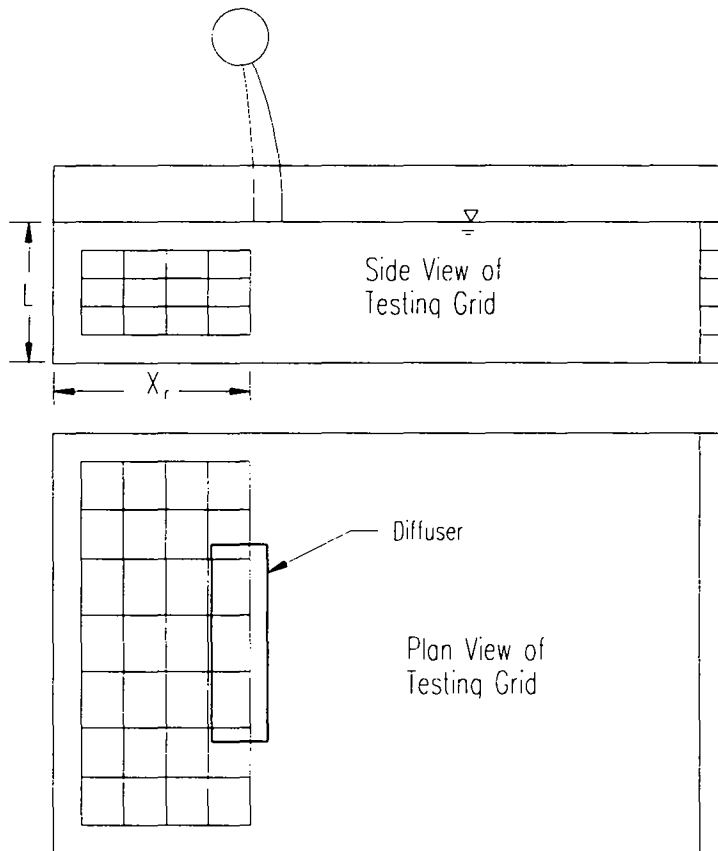


**Figure 3.16: ADV Testing Grid**

The test procedures are summarized as follows:

1. Place stop logs to create desired tailwater level
2. Set discharge
3. Measure tailwater level at desired locations
4. Measure jet location and dimensions at impact
5. Prepare data collection sheets
6. Bleed air from all tubing on the transducer board
7. Measure back-flushing pitot tube baseline voltage
8. Collect back-flushing pitot tube data
9. Calibrate air concentration probe
10. Collect air concentration data
11. Calibrate ADV
12. Collect ADV data
13. Transform ADV binary file into ASCII data

## CHAPTER 4

### RESULTS & DATA ANALYSIS

Data were collected using the back-flushing pitot tube, air concentration probe, and ADV. Variables measured during each test include velocity at impact, air concentration at impact, and velocity magnitude and flow direction throughout the roller region. Test results and data analysis are presented.

#### 4.1 Data Reduction

Five time-averaged velocities were recorded with the back-flushing pitot tube and air concentration probe along the jet width at the impact plane with the water surface as indicated in Figure 3.15. The time-averaged velocity of the jet at impact with the surface of the plunge pool ( $V_j$ ) is the average of the five impact velocity measurements. The average adjusted air concentration ( $A$ ) is obtained from the air concentration probe measurements taken at the same five impact locations along the impact plane. Table 4.1 summarizes the tailwater depths and jet characteristics at impact for each test.

Table 4.1: Impact Data

Test No.	Width Ratio	Flow Rate	No. of Stop Logs	Depth in Roller Region	Depth Down-stream	Impact Air Concentration	Impact Velocity
	$W$	$Q$		$L$	$L_d$	$A$	$V_i$
		(m <sup>3</sup> /s)	(#)	(m)	(m)	(%)	(m/s)
01	3:1	0.085	1	0.49	0.49	68.57	3.31
02	3:1	0.085	5	0.82	0.82	74.09	4.23
03	3:1	0.085	8	1.07	1.06	72.37	3.92
04	3:1	0.142	1	0.49	0.49	85.56	4.94
05	3:1	0.142	5	0.84	0.83	84.26	4.94
06	3:1	0.142	8	1.10	1.09	81.04	5.34
07	1:1	0.085	1	0.49	0.49	81.65	4.65
08	1:1	0.085	5	0.82	0.81	74.24	3.95
09	1:1	0.085	8	1.06	1.05	70.35	3.88
10	1:1	0.142	1	0.51	0.52	86.77	5.07
11	1:1	0.142	5	0.84	0.83	84.66	5.25
12	1:1	0.142	8	1.08	1.08	79.36	4.83
13	1:1	0.113	1	0.49	0.49	81.60	4.53
14	1:1	0.113	5	0.83	0.82	74.51	4.13
15	1:1	0.113	8	1.07	1.06	71.83	3.55
16	3:1	0.113	1	0.49	0.48	82.50	4.71
17	3:1	0.113	5	0.82	0.82	81.55	4.44
18	3:1	0.113	8	1.08	1.07	80.29	4.62
19	1:2	0.085	1	0.48	0.48	81.69	4.28
20	1:2	0.085	5	0.82	0.82	66.74	3.36
21	1:2	0.085	8	1.06	1.06	75.54	4.20
22	1:2	0.113	1	0.49	0.49	82.24	3.66
23	1:2	0.113	5	0.83	0.82	77.12	4.31
24	1:2	0.113	8	1.08	1.07	79.06	5.07
25	1:2	0.142	1	0.49	0.49	84.28	4.59
26	1:2	0.142	5	0.84	0.83	80.27	4.88
27	1:2	0.142	8	1.08	1.07	78.06	5.50

The ADV measured the time-averaged velocity components,  $V_x$ ,  $V_y$ , and  $V_z$ , at each location of the testing grid in the roller region. SonTek® software was used to record ADV data and convert the data from binary to ASCII. The ADV output for each test is presented in Section 4.3.4. Two-dimensional (2-D) velocity vectors in any of the three planes, XY, XZ, or YZ, may be calculated from the velocity components.

#### 4.2 Flow Patterns

The general flow patterns for each test remained constant and are presented in Figure 4.1. The vortex in the plunge pool on the upstream side of the jet at impact

(roller region) shown in Figure 4.1 is defined as having a counter-clockwise (downstream flow is left to right) rotation. The direction of the circulating flow in the roller region is contrary to previous perceptions (Cola, 1965, Jirka and Harleman, 1979). The circulation direction shown in Figure 4.1 may result in sediment degradation near the toe of the dam rather than sediment aggradation as previously believed. All of the tests in this study produced vortices rotating in the counter-clockwise direction.

The flow pattern produced by the free falling, developed jet indicates that flow circulates upstream of the jet impact region on the surface, vertically down into the plunge pool at the back wall, downstream along the floor, and out of the basin. Flow patterns varied slightly with changes in tailwater depth in the roller region; the flow pattern of the vortex became elongated as the tailwater depth decreased. A decrease in the lateral width of the basin (canyon width) caused an increase in the magnitude of the velocity vectors. The Marsh-McBirney® velocity meter verified the velocity and flow direction data acquired using the ADV.

The  $V_x$  and  $V_z$  velocity components recorded by the ADV were combined producing 2-D vectors in the XZ plane. Axum® graphing software produced a visual display of the flow pattern occurring in the roller region. Figure 4.2 is an Axum® graph which portrays the velocity vectors in one XZ plane located in the roller region.

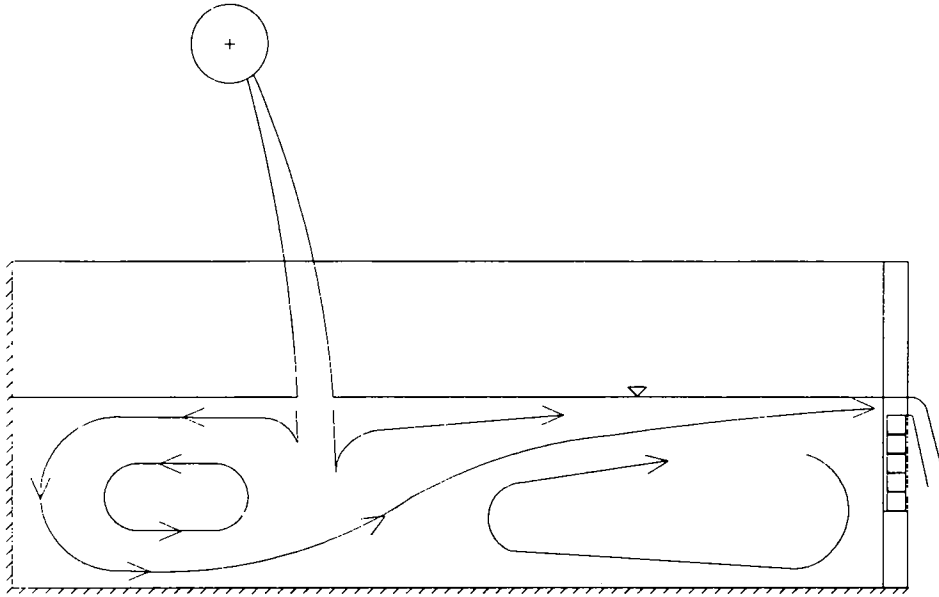


**Figure 4.1: General Flow Patterns**

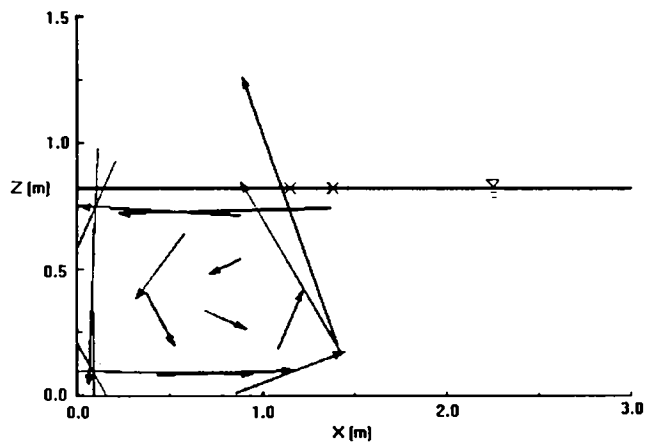


**Figure 4.2: Flow Pattern Example**

Each arrow in the plot depicts both the direction and magnitude of the velocity vector at a specific location. The center of the arrow is located at the data collection coordinates, while the length of each arrow is relative to the magnitude of the velocity.

The horizontal line represents the free surface and the crosses represent the upstream and downstream limits of the jet at impact. Mapping of the data allowed visual comparison of the flow patterns produced by varying test conditions.

Three factors are attributed to the counter-clockwise rotation of the vortex in the roller region as illustrated in Figure 4.3. The first factor is the rebound effect. A stagnation point occurs at the interface between the plunging jet and the return flow as illustrated in Figure 4.3. Return flow is the flow along the floor which continues downstream rather than turning upward following the circulation path. As the jet travels into the basin and approaches the floor, the impact of the jet with the stagnation zone above the floor causes the fluid to rebound in an upward direction. The rebound effect occurs in the impact region near the floor, yet the force of the incoming jet prevents flow from rebounding directly into the incoming flow of the jet. Thus, the rebound occurs at the edges of the jet impact region. The rebound effect is discussed by Cola (1965), Lencastre (George, 1980), and Lee and Jirka (1981). As the tailwater depth increases, the significance of the rebound decreases. When the tailwater depth is sufficient that complete diffusion of the jet occurs prior to impact near the basin floor, the rebound no longer occurs.

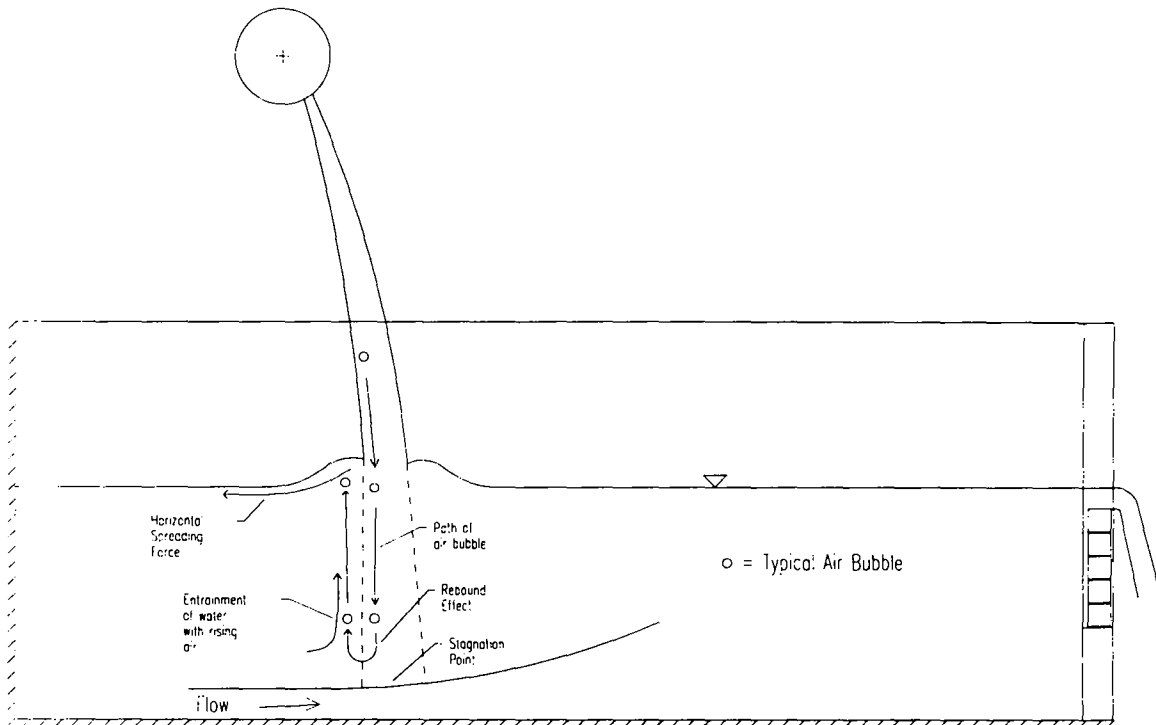


**Figure 4.3: Circulation Driving Forces**

The second, and most significant factor leading to the counter-clockwise rotating vortex is the buoyancy force resulting from the high degree of air entrainment in the plunging jet. When a highly turbulent and aerated jet impacts a free surface, additional air is entrained into the flow. The buoyancy force produced by the air entrainment is directed upward and causes the velocities in the jet region to decrease at a greater rate than if the jet had negligible air entrainment. The increased rate of velocity decay of plunging jets due to aeration is discussed by Bohrer (1996). The significance of buoyancy forces in jets has been reported by Cola (1965), Jirka and Harleman (1979), and Lee and Jirka (1981). Cola noted that under certain conditions, the buoyancy force was greater than the force of the jet. Lee and Jirka (1981) and Jirka and Harleman (1979) documented that buoyancy is the crucial factor in determining the stability of

circulating flow. Ervine and Falvey (1987), Breusers (1991), and Bohrer (1996) documented the effect air entrainment on reducing velocities and pressures on the basin floor in the jet region.

When the air entrained in the jet is forced outside of the jet region by the incoming jet, the air flows upward toward the free surface along the jet region perimeter. The rising air causes fluid outside of the jet region to be drawn upwards. The combination of the rebound effect and the buoyancy force of the impinging jet results in air and water flowing towards the water surface along the jet boundary. Boils at the water surface indicate the strength of the upward force created by the rebound effect and buoyancy force resultant. The boils cause a super-elevation of the water surface similar to those documented by Lee and Jirka (1981).

A third driving force affecting the direction of circulation is the horizontal spreading of flow on the surface of the water created by the impacting jet as documented by Lee and Jirka (1981). Rebounding flow, the buoyancy force, and horizontal spreading of surface flow become the driving forces for the counter-clockwise rotating vortex in the roller region.

#### 4.3 Velocity Prediction Equations

A method for predicting the velocities in specific zones of the plunge pool is desired to determine the erosion potential of the circulating flow. A dimensional analysis was performed to determine the critical variables required for velocity prediction in the roller region where impact velocity, impact air concentration, jet width, basin (canyon) width, and gravitational acceleration were considered the primary

variables. Statistical and regression analyses were also performed in order to yield accurate prediction equations.

#### 4.3.1 Velocity Component and Vector Comparison

The velocity components in the circulation pattern acquired by the ADV are used to calculate the velocity vectors in any of the three planes. At the back wall zone, the  $V_z$  component is the major component, while  $V_x$  is the major component in the floor zone. When the major component at a location is combined with its corresponding minor component, the resulting vector will be greater in magnitude than either of its components. The maximum vector in a zone for a specific condition is not always at the same location as the maximum major velocity component. This is due to the fact that both the major and minor components produce the vector. If a location has a very large major component and a very small minor component, the resulting vector may be smaller in magnitude than a vector produced by a slightly smaller major component and slightly larger minor component.

It is advised that when performing predictive calculations, the maximum velocity vector prediction equations be used as opposed to the velocity component prediction equations. The velocity vector represents flow velocity more ideally than using one velocity component. Also, the use of the maximum velocity vector rather than the average velocity vector or a velocity component will yield conservative values when calculating stream power and erosion potential.

#### 4.3.2 Dimensional Analysis

An analysis of the circulation velocities in the roller region was conducted. Prediction of the velocities in the roller region was accomplished using nondimensional

quantities so that the results may be scaled and applied to a prototype or field condition. Trends in the velocities were examined with respect to dimensionless groups. Using the Buckingham Pi Theorem, a form of the densimetric Froude number used by Jirka and Harleman (1979) and Lee and Jirka (1981) was determined to be an important nondimensional quantity in describing the velocities in the roller region and is expressed as:

$$\Pi_1 = A * W * \frac{V_i}{\sqrt{g * L}} \quad (4.1)$$

where

- $\Pi_1$  = Dimensionless group
- $A$  = Air concentration (decimal)
- $W$  = Ratio of canyon width to jet width
- $V_i$  = Velocity at impact (m/s)
- $g$  = Gravitational acceleration (m/s<sup>2</sup>)
- $L$  = Depth in roller region (m)

In order to transform the velocity components and vectors in the roller region into dimensionless quantities, a second nondimensional group was derived:

$$\Pi_2 = \pm 0.01 * \frac{V'}{V_i} \quad (4.2)$$

where

- $\Pi_2$  = Dimensionless group
- $V'$  = Velocity component or vector as identified (cm/s)  
i.e.,:  $V_x$  is the X component of the 3-D velocity vector  
 $V_{xz}$  is the 2-D velocity vector in the XZ plane
- $V_i$  = Velocity at impact (m/s)

When calculating  $\Pi_2$ ,  $V'$  must have units of cm/s, while  $V_i$  must have units of m/s. The factor of 0.01 in Equation 4.2 converts ADV output of centimeters to meters. The

negative sign converts the negative  $V_z$  velocity components into positive values for graphic purposes.  $V$  will be replaced with  $V_{xz\_max}$  when implementing the prediction procedure discussed in Chapter 5.

### 4.3.3 Critical Zones

Velocity data were collected throughout the roller region for each test. The two critical zones in the model are defined as the “back wall” and “floor” zones. These two zones represent the dam face and the plunge pool floor; locations where understanding scour potential is crucial. Each zone, as illustrated in Figure 4.4, is a three dimensional control volume and has the following boundaries:

Back wall zone boundaries:

X-direction: From the back wall to  $0.10 X_r$

Y-direction: Zone width equals the jet width at impact

Z-direction:  $0.20 L$  to  $0.80 L$

Floor zone boundaries:

X-direction:  $0.10 X_r$  to  $0.85 X_r$

Y-direction: Zone width equals the jet width at impact

Z-direction: From the floor to  $0.20 L$

where

$L$  = Depth in the roller region (L)

$X_r$  = Distance from upstream boundary to upstream side of jet at impact (L)

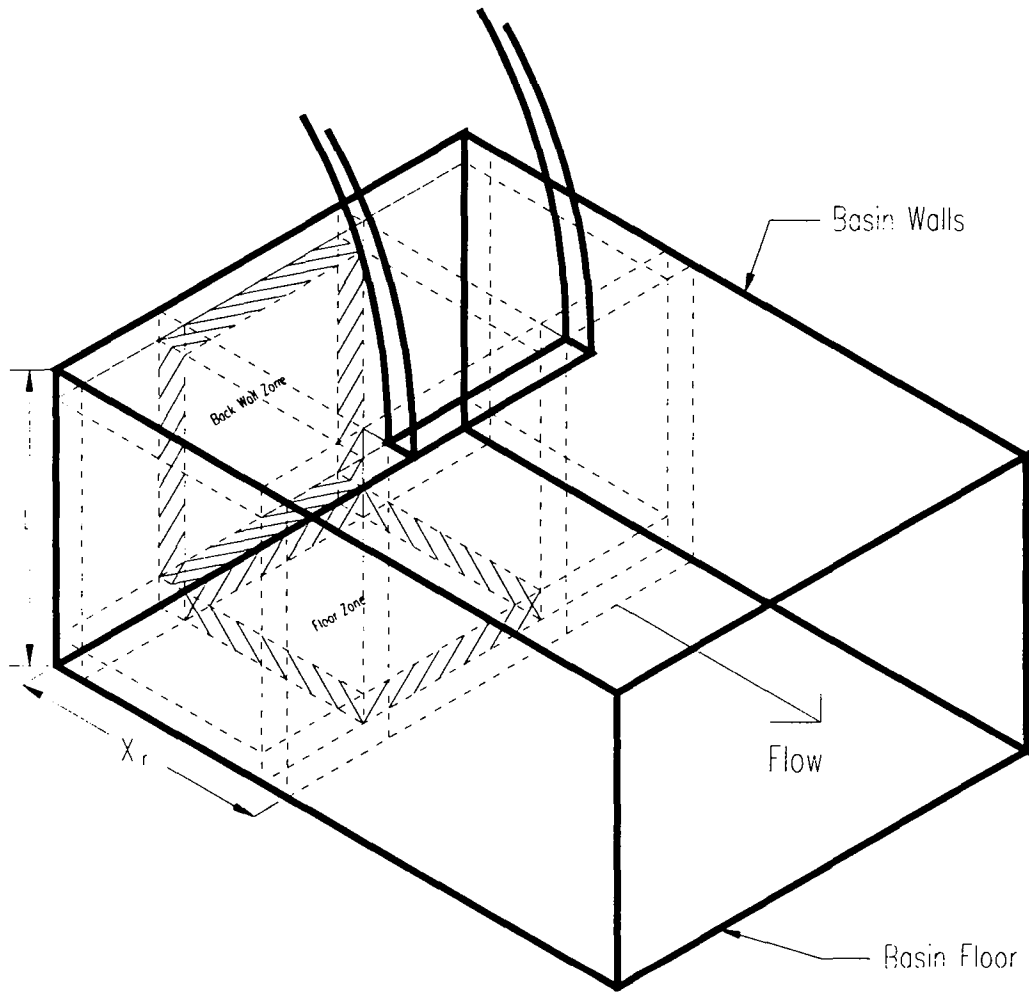


**Figure 4.4: Zone Boundaries**

#### 4.3.4 Data Analysis

The coordinate system defined the positive X-direction to be downstream and the positive Z-direction to be vertically upward. Flow from the counter-clockwise rotating vortex produces a velocity down the back wall which is represented by a negative Vz value. The velocity components in the X-direction and Z-direction produce the velocity vectors in the XZ plane. For the back wall zone, the Vz velocity component is much greater than the Vx component. In the floor zone, the Vx velocity component is much greater than the Vz component. The major component is typically at least three times larger than the minor component, however, it is not uncommon for the major component to be hundreds of times larger than the minor component when the magnitude of the minor component approaches zero. On average, the major component is ten to twenty times larger than the minor component. Section 4.3.6 presents detailed comparisons of the velocity magnitudes.

Velocity data for the back wall and floor zones were analyzed. Processing the velocity data consisted of extracting the data for each of the back wall and floor zones and then calculating the minimum, maximum, average, and standard deviation values of the velocity components. For example, if eight grid intersections are located in the back wall zone, then there are eight velocity components in the Z-direction. Of the eight values, one of the velocity components is the maximum, one is the minimum, and all eight values are used to determine the average velocity and standard deviation. The results of the statistical analysis for the velocity components in the X-direction and Z-direction at the back wall and floor are presented in Table 4.2 and Table 4.3. Also presented are the ratio of the average to minimum value for the Vz component at the

back wall and the ratio of the average to maximum value for the Vx component at the floor. The Vz minimum is the maximum value in the negative Z-direction. Table 4.4 summarizes the results of the statistical analysis for the velocity components in both the back wall and floor zones.

#### 4.3.5 Regression Analysis

A regression analysis was performed on the data for all tests using the following methods: linear, logarithmic, polynomial, power, exponential, and moving average. Natural log based regression equations best describe the relationship between the data and the dimensionless groups based on the coefficients of determination. Figure 4.5 through Figure 4.8 present the following velocity component data: Vz\_min and Vz\_avg at the back wall for the three width ratios and Vx\_max and Vx\_avg at the floor for the three width ratios. Figure 4.9 through Figure 4.12 present the Vxz\_max and Vxz\_avg velocity vector data for the three width ratios at the back wall and floor zones. The horizontal axis for Figure 4.5 through Figure 4.12 is the densimetric Froude number,  $\Pi_1$ , excluding the width ratio,  $W$ .

**Table 4.2: Back Wall Zone Velocity Component Data**

Test No.	Width Ratio <i>W</i>	Flow Rate <i>Q</i> (m <sup>3</sup> /s)	Roller Depth <i>L</i> (m)	Back Wall Zone (Major component: <i>V<sub>z</sub></i> )								
				<i>V<sub>x</sub></i>				<i>V<sub>z</sub></i>				
				Min. (cm/s)	Max. (cm/s)	Avg. (cm/s)	Std. Dev.	Min. (cm/s)	Max. (cm/s)	Avg. (cm/s)	Std. Dev.	Avg./Min.
01	3:1	0.085	0.49	-4.03	3.52	-1.24	2.42	-16.59	-5.30	-10.09	3.35	0.61
02	3:1	0.085	0.82	-2.92	3.68	-0.33	2.27	-16.38	-7.67	-12.06	2.80	0.74
03	3:1	0.085	1.07	-2.04	5.77	0.84	2.65	-16.82	-11.84	-14.82	1.36	0.88
04	3:1	0.142	0.49	-2.75	5.52	1.99	2.81	-4.96	-2.27	-3.63	1.12	0.73
05	3:1	0.142	0.84	0.82	4.91	2.70	1.61	-9.54	-4.96	-7.23	1.65	0.76
06	3:1	0.142	1.10	1.19	6.67	2.59	1.90	-9.25	-5.63	-7.15	1.36	0.77
07	1:1	0.085	0.49	-12.10	10.01	0.58	7.35	-27.17	-10.99	-19.35	5.19	0.71
08	1:1	0.085	0.82	-3.04	8.56	2.65	3.95	-38.88	-13.92	-29.53	7.46	0.76
09	1:1	0.085	1.06	-6.18	2.50	0.06	2.89	-36.80	-13.77	-28.30	7.35	0.77
10	1:1	0.142	0.51	-7.70	4.61	-2.66	4.55	-23.08	-3.75	-16.62	6.69	0.72
11	1:1	0.142	0.84	-11.88	7.56	-1.32	5.79	-36.67	-5.38	-22.95	11.06	0.63
12	1:1	0.142	1.08	-6.24	5.63	-0.23	3.69	-38.91	-8.35	-23.62	11.80	0.61
13	1:1	0.113	0.49	-11.69	6.23	-2.49	5.27	-22.93	-8.35	-17.13	5.15	0.75
14	1:1	0.113	0.83	-8.29	8.60	0.56	5.65	-38.69	-8.47	-26.03	9.42	0.67
15	1:1	0.113	1.07	-6.38	5.51	-0.27	3.70	-36.01	-11.95	-25.20	8.66	0.70
16	3:1	0.113	0.49	-0.92	0.28	-0.18	0.45	-10.02	-7.27	-8.45	1.14	0.84
17	3:1	0.113	0.82	-0.42	0.92	0.48	0.53	-13.26	-8.56	-11.06	1.84	0.83
18	3:1	0.113	1.08	0.17	1.56	0.86	0.50	-13.84	-9.86	-11.74	1.49	0.85
19	2:1	0.085	0.48	-0.91	7.18	3.08	2.95	-15.25	0.21	-10.87	6.45	0.71
20	2:1	0.085	0.82	-2.38	5.91	1.68	2.64	-26.61	-10.13	-17.50	5.44	0.66
21	2:1	0.085	1.06	0.32	4.16	2.16	1.46	-29.21	-14.26	-19.41	5.89	0.66
22	2:1	0.113	0.49	-2.10	4.76	0.66	2.86	-22.04	-0.78	-13.12	8.07	0.60
23	2:1	0.113	0.83	-5.66	3.46	-0.56	2.57	-35.49	-9.63	-23.98	8.70	0.68
24	2:1	0.113	1.08	-3.88	2.80	0.14	2.07	-35.76	-10.58	-23.14	8.55	0.65
25	2:1	0.142	0.49	-2.89	-0.77	-1.51	0.84	-23.75	-7.85	-15.59	6.48	0.66
26	2:1	0.142	0.84	-7.48	2.00	-1.57	3.10	-37.67	-0.42	-22.63	12.10	0.60
27	2:1	0.142	1.08	-6.49	2.65	-0.55	2.74	-38.85	-5.35	-23.75	10.87	0.61

**Table 4.3: Floor Zone Velocity Component Data**

Test No.	Width Ratio	Flow Rate	Roller Depth	Floor Zone (Major component: Vx)								
				Vx					Vz			
				W	Q	L	Min.	Max.	Avg.	Std. Dev.	Avg./Max	Min.
	(m3/s)	(m)	(cm/s)	(cm/s)	(cm/s)		(cm/s)	(cm/s)	(cm/s)			
01	3:1	0.085	0.49	5.86	17.50	10.86	3.52	0.62	-0.50	3.23	1.15	1.49
02	3:1	0.085	0.82	8.26	17.81	12.77	3.32	0.72	-0.70	5.70	3.21	2.09
03	3:1	0.085	1.07	9.75	18.28	13.29	3.14	0.73	2.91	3.76	3.31	0.31
04	3:1	0.142	0.49	5.21	18.92	11.73	4.09	0.62	-2.55	4.20	0.83	1.88
05	3:1	0.142	0.84	15.36	18.09	16.32	1.07	0.90	-2.73	-1.37	-1.95	0.50
06	3:1	0.142	1.10	11.72	16.31	14.12	1.36	0.87	-2.71	0.97	-0.88	1.24
07	1:1	0.085	0.49	15.39	32.07	24.73	5.15	0.77	-5.93	11.04	2.54	4.73
08	1:1	0.085	0.82	28.56	39.57	33.43	3.80	0.84	-5.65	8.45	1.39	3.86
09	1:1	0.085	1.06	11.40	35.74	27.28	7.39	0.76	-5.18	10.89	0.73	5.09
10	1:1	0.142	0.51	0.52	31.90	21.77	12.33	0.68	-5.13	15.15	2.77	6.01
11	1:1	0.142	0.84	19.36	47.35	29.00	8.07	0.61	-3.96	9.83	1.40	4.29
12	1:1	0.142	1.08	-15.85	42.51	22.08	16.47	0.52	-4.69	7.01	1.10	4.19
13	1:1	0.113	0.49	12.73	32.93	23.59	6.85	0.72	-1.65	8.02	3.59	3.04
14	1:1	0.113	0.83	23.09	45.28	31.66	6.16	0.70	-4.68	8.38	0.64	3.79
15	1:1	0.113	1.07	-9.46	38.76	24.36	14.48	0.63	-6.53	9.42	1.40	5.41
16	3:1	0.113	0.49	0.57	12.86	9.22	3.72	0.72	-2.19	3.08	0.61	1.63
17	3:1	0.113	0.82	4.35	22.71	14.30	6.25	0.63	-1.02	4.16	2.30	1.74
18	3:1	0.113	1.08	8.59	19.83	14.38	3.36	0.73	-2.08	3.96	1.80	1.86
19	2:1	0.085	0.48	0.39	25.92	19.18	7.88	0.74	-2.55	8.32	2.31	3.66
20	2:1	0.085	0.82	20.61	29.25	24.86	3.00	0.85	-4.34	6.24	0.83	3.43
21	2:1	0.085	1.06	17.51	25.78	21.01	2.48	0.82	-5.20	6.37	-0.19	3.48
22	2:1	0.113	0.49	14.52	26.44	21.46	3.80	0.81	-3.50	9.59	1.69	4.31
23	2:1	0.113	0.83	22.40	31.76	26.14	2.93	0.82	-5.05	4.70	-0.33	3.55
24	2:1	0.113	1.08	20.78	26.96	23.67	2.39	0.88	-5.75	4.12	-0.42	3.49
25	2:1	0.142	0.49	16.05	25.18	21.10	2.94	0.84	-3.07	7.45	0.96	3.48
26	2:1	0.142	0.84	20.12	27.42	22.95	2.14	0.84	-4.13	5.19	-0.05	3.22
27	2:1	0.142	1.08	19.42	24.81	22.03	1.87	0.89	-5.54	3.65	-0.54	3.06

**Table 4.4: Velocity Vector Data**

Test No.	Width Ratio	Flow Rate	Roller Depth	Vxz - Back Wall Zone					Vxz - Floor Zone				
				W	Q (m <sup>3</sup> /s)	L (m)	Min. (cm/s)	Max. (cm/s)	Avg. (cm/s)	Std. Dev. (cm/s)	Avg./Max.	Min. (cm/s)	Max. (cm/s)
01	3:1	0.085	0.49	6.60	17.07	10.50	3.20	0.61	6.55	17.50	11.09	3.31	0.63
02	3:1	0.085	0.82	8.21	16.48	12.30	2.68	0.75	9.45	18.04	13.42	2.96	0.74
03	3:1	0.085	1.07	11.86	17.46	15.07	1.49	0.86	10.45	18.59	13.72	3.03	0.74
04	3:1	0.142	0.49	2.76	6.15	5.01	1.07	0.81	6.69	18.97	12.00	3.81	0.63
05	3:1	0.142	0.84	5.40	10.60	7.90	1.58	0.74	15.48	18.17	16.45	1.03	0.91
06	3:1	0.142	1.10	6.16	11.40	7.73	1.89	0.68	12.03	16.33	14.21	1.28	0.87
07	1:1	0.085	0.49	13.91	29.74	20.81	4.78	0.70	16.49	32.07	25.36	4.86	0.79
08	1:1	0.085	0.82	15.49	39.00	30.03	6.95	0.77	28.86	39.57	33.70	3.67	0.85
09	1:1	0.085	1.06	13.87	37.31	28.44	7.40	0.76	15.77	36.12	28.01	6.35	0.78
10	1:1	0.142	0.51	7.66	23.93	17.85	5.47	0.75	1.16	32.80	23.89	9.96	0.73
11	1:1	0.142	0.84	6.77	38.55	23.74	10.98	0.62	19.38	47.46	29.41	7.84	0.62
12	1:1	0.142	1.08	8.55	39.08	23.98	11.65	0.61	13.84	42.77	26.39	8.99	0.62
13	1:1	0.113	0.49	9.88	23.75	18.12	5.06	0.76	14.21	33.14	24.12	6.64	0.73
14	1:1	0.113	0.83	10.86	39.57	26.83	8.88	0.68	23.13	45.32	31.91	6.05	0.70
15	1:1	0.113	1.07	13.16	36.09	25.51	8.55	0.71	13.35	39.41	27.56	8.66	0.70
16	3:1	0.113	0.49	7.33	10.03	8.47	1.13	0.84	0.73	13.06	9.40	3.67	0.72
17	3:1	0.113	0.82	8.60	13.29	11.08	1.84	0.83	5.79	22.87	14.78	5.77	0.65
18	3:1	0.113	1.08	9.98	13.86	11.79	1.45	0.85	8.88	20.08	14.61	3.33	0.73
19	2:1	0.085	0.48	7.18	15.79	12.90	3.44	0.82	4.66	26.12	20.13	6.58	0.77
20	2:1	0.113	0.82	10.76	26.73	17.83	5.23	0.67	20.76	29.54	25.10	3.08	0.85
21	2:1	0.142	1.06	14.86	29.24	19.62	5.77	0.67	17.68	25.87	21.29	2.56	0.82
22	2:1	0.085	0.49	4.82	22.12	14.22	6.60	0.64	17.40	26.79	22.04	3.28	0.82
23	2:1	0.113	0.83	9.63	35.94	24.11	8.75	0.67	22.46	32.11	26.38	2.97	0.82
24	2:1	0.142	1.08	10.76	35.97	23.23	8.56	0.65	20.96	27.27	23.93	2.38	0.88
25	2:1	0.085	0.49	7.99	23.92	15.68	6.49	0.66	16.05	25.32	21.42	2.85	0.85
26	2:1	0.113	0.84	0.50	38.41	22.83	12.22	0.59	20.39	27.90	23.17	2.23	0.83
27	2:1	0.142	1.08	5.47	39.39	23.89	10.91	0.61	19.46	25.08	22.25	1.93	0.89

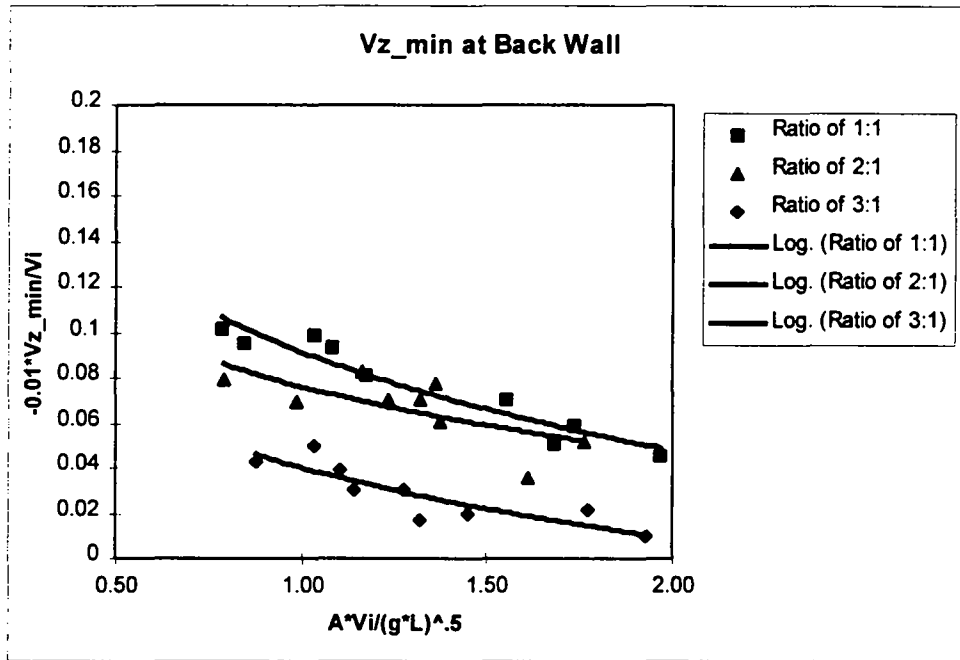


**Figure 4.5: Vz\_min at Back Wall**

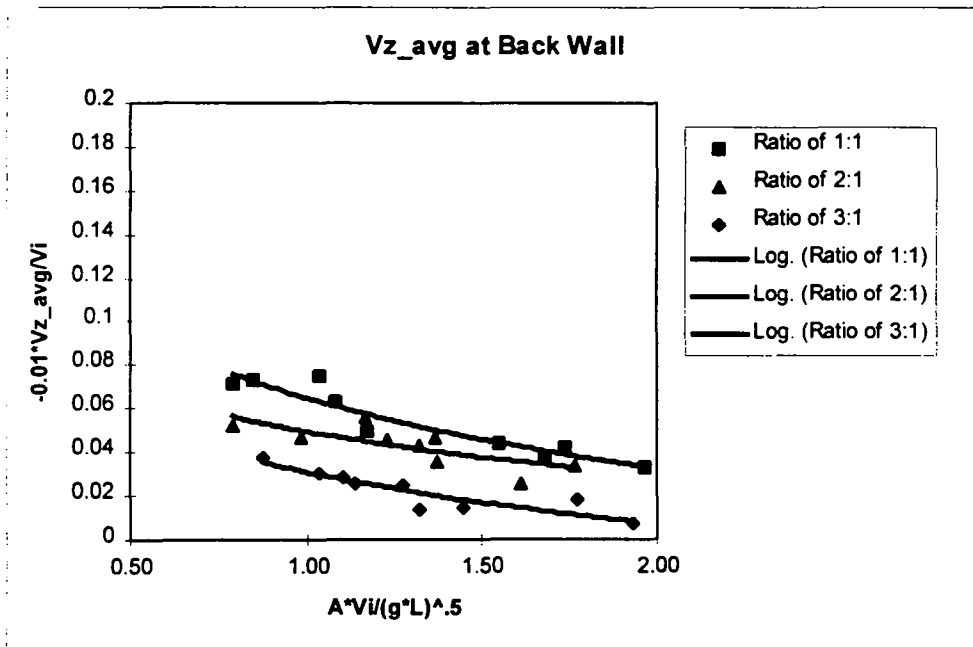


**Figure 4.6: Vz\_avg at Back Wall**

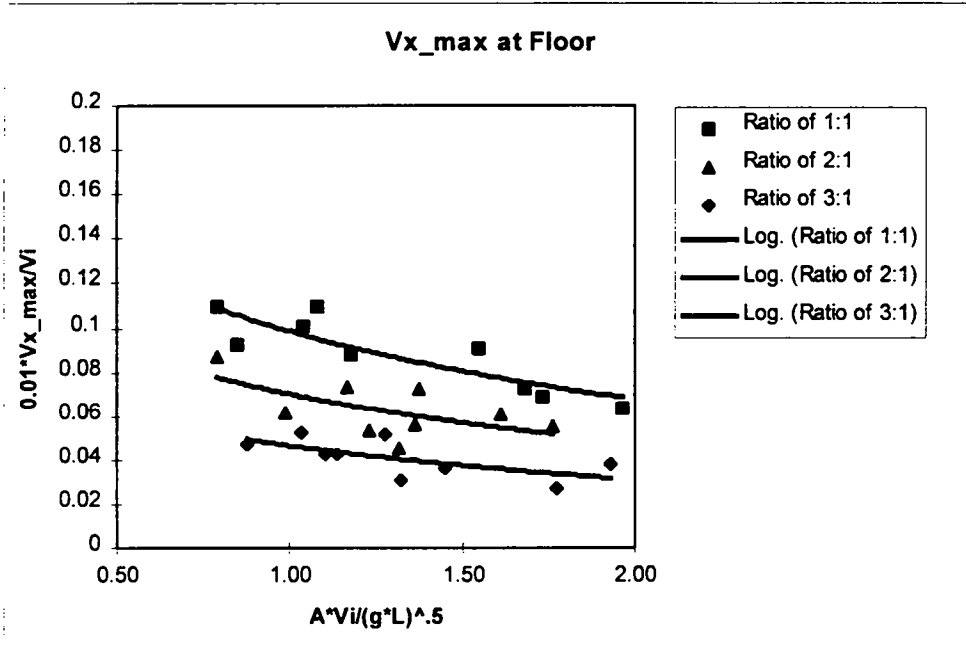


**Figure 4.7: Vx\_max at Floor**

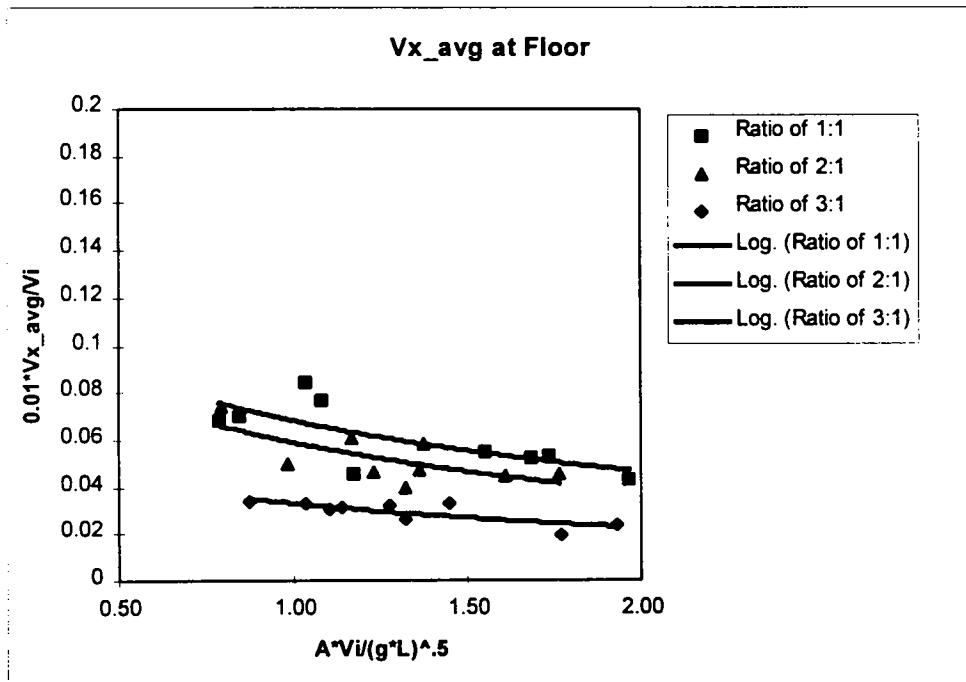


**Figure 4.8: Vx\_avg at Floor**

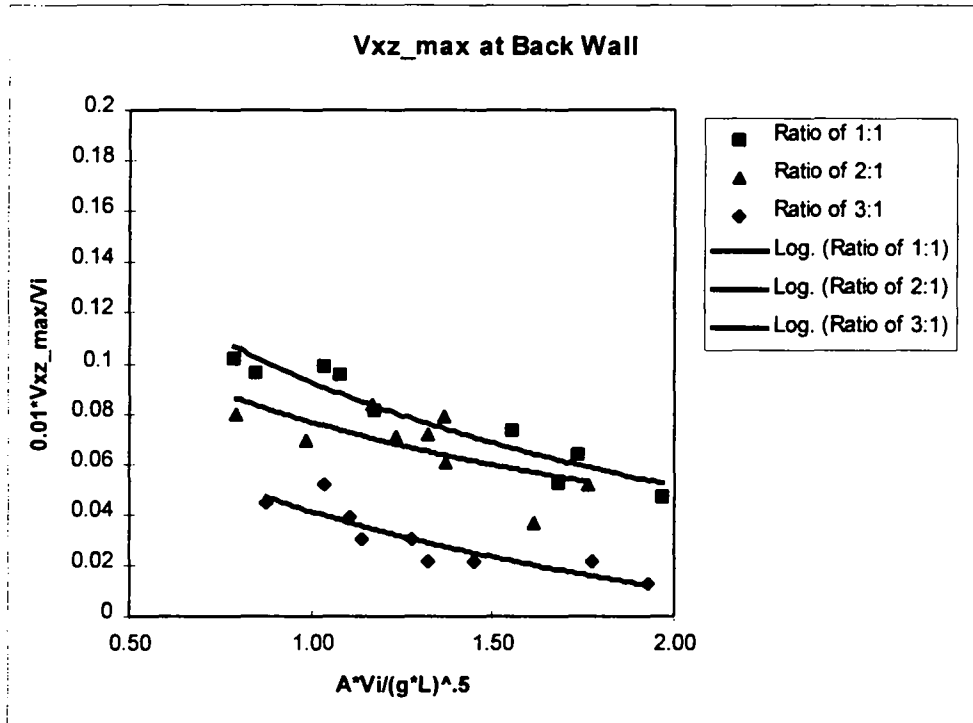


**Figure 4.9: Vxz\_max at Back Wall**

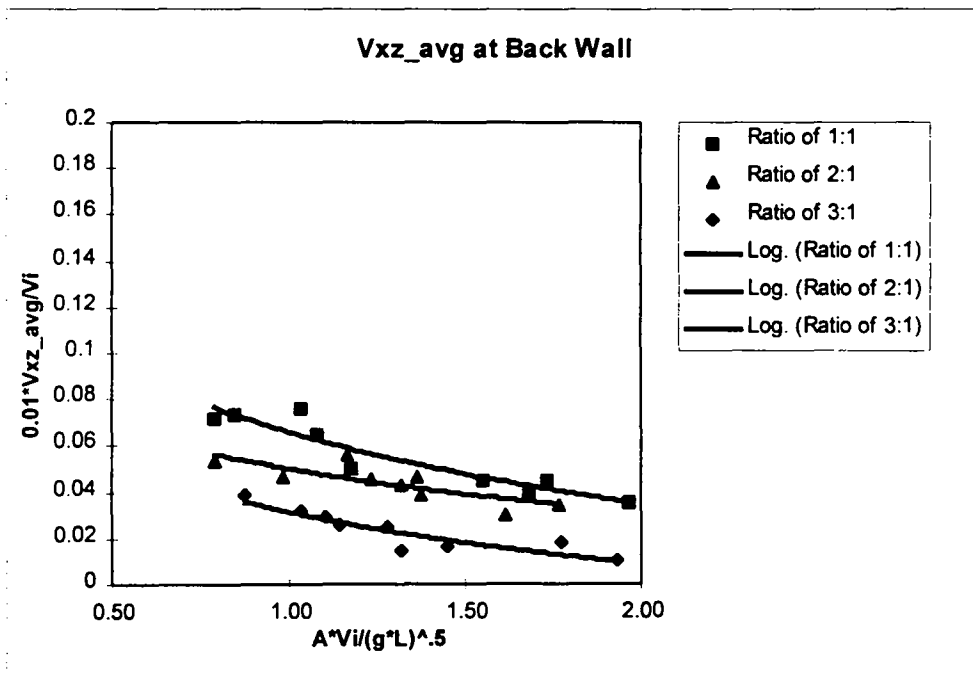


**Figure 4.10: Vxz\_avg at Back Wall**

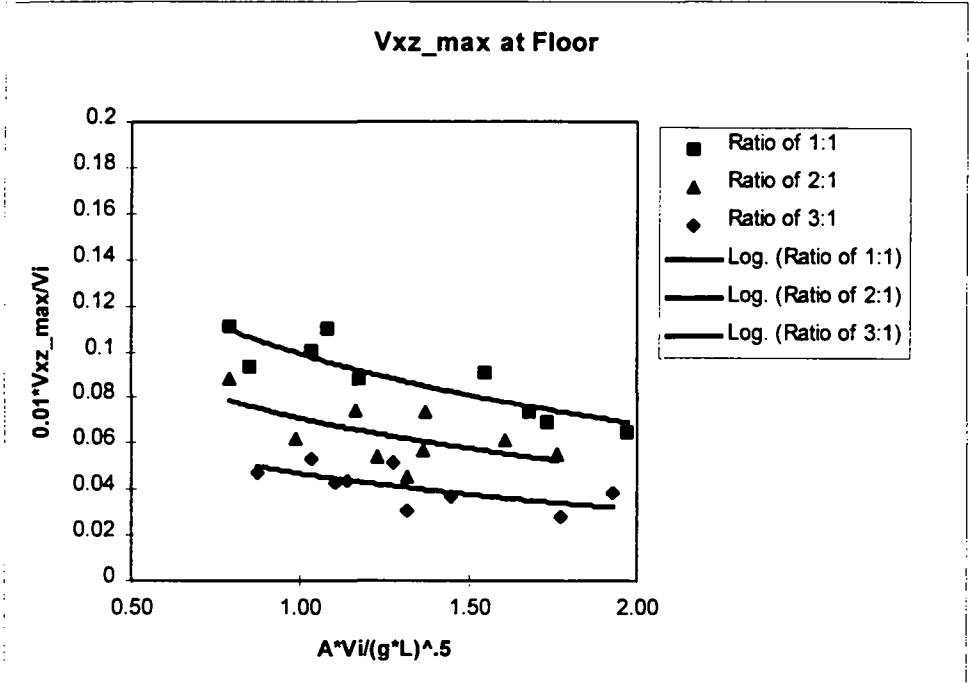


Figure 4.11:  $V_{xz\_max}$  at Floor

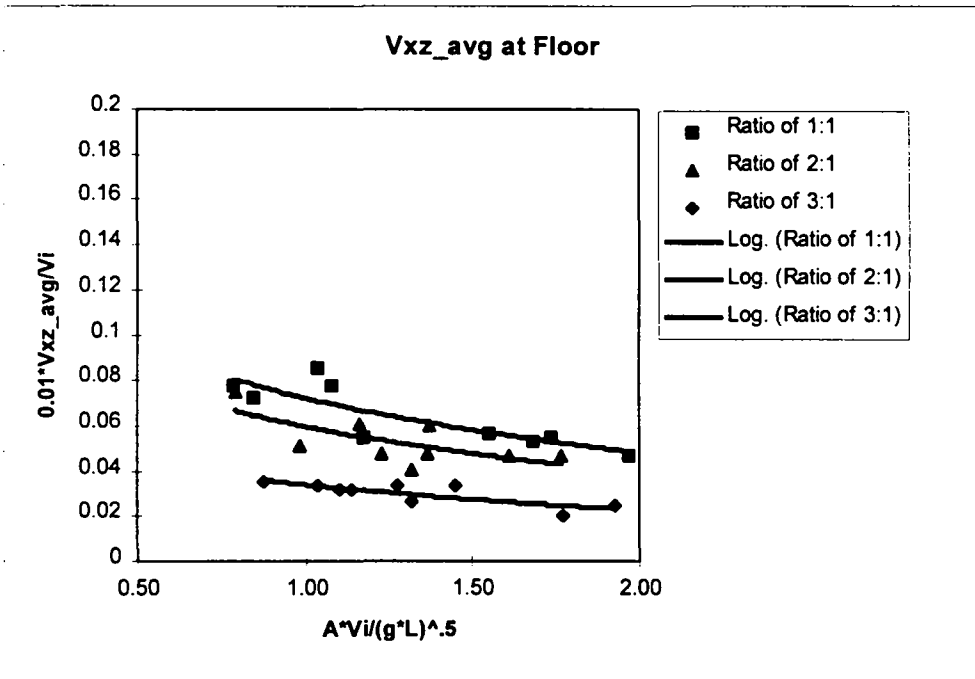
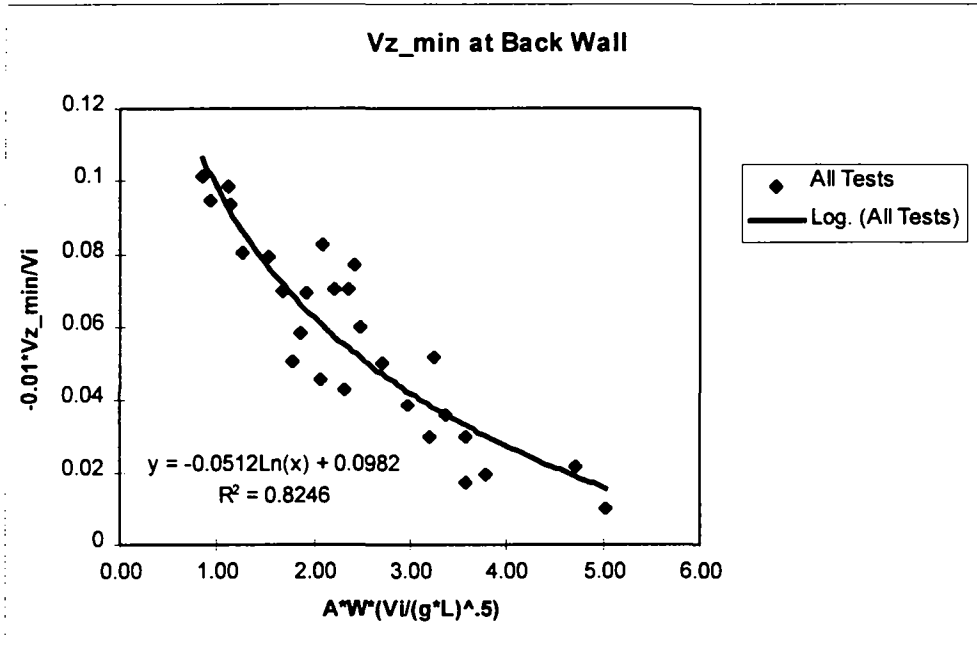


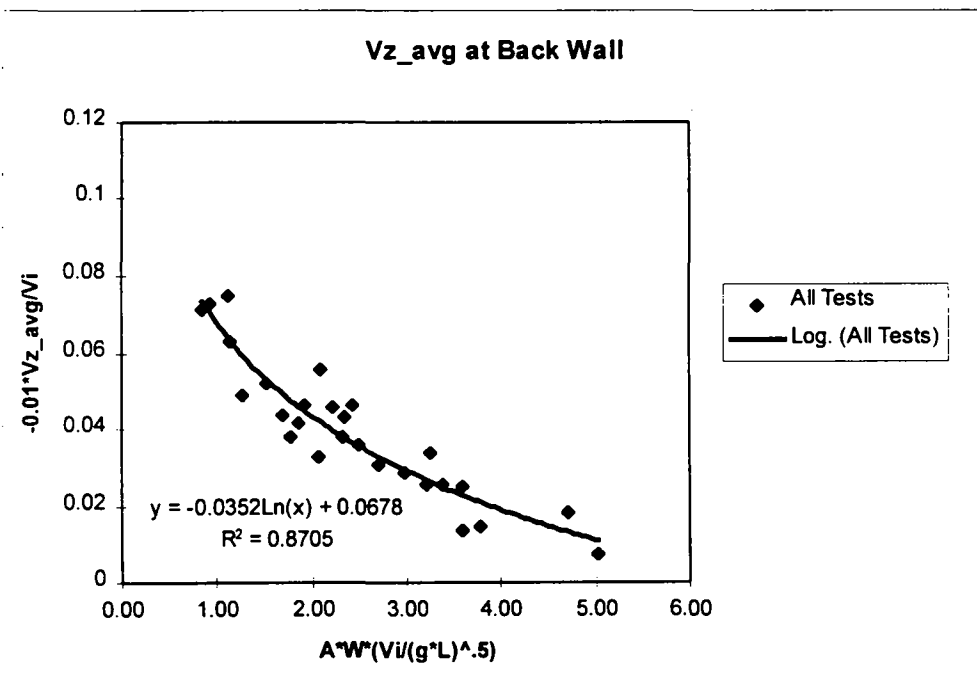
Figure 4.12:  $V_{xz\_avg}$  at Floor

Figure 4.5 through Figure 4.12 demonstrate that a change in the canyon width greatly changes the magnitude of the velocities in the circulation pattern. As the canyon width is decreased, an increase in the circulation velocities results. A detailed comparison of the velocity magnitudes is presented in section 4.3.6.

In order to describe velocity component or velocity vector data at a specified zone for the three width ratios using a single equation,  $\Pi_1$  (Equation 4.1) was introduced as the dimensionless quantity on the horizontal axis. The width ratio,  $W$ , was found to be a significant variable which collapses the data while retaining high coefficients of determination. The velocity data are plotted against the dimensionless groups,  $\Pi_1$  and  $\Pi_2$ . Plots of  $Vz\_min$  and  $Vz\_avg$  at the back wall zone and  $Vx\_max$  and  $Vx\_avg$  at the floor zone are presented in Figure 4.13 through Figure 4.16. Plots of the maximum and average  $Vxz$  velocity vector at the back wall and floor zones are presented in Figure 4.17 through Figure 4.20.



**Figure 4.13: Vz\_min at Back Wall**



**Figure 4.14: Vz\_avg at Back Wall**

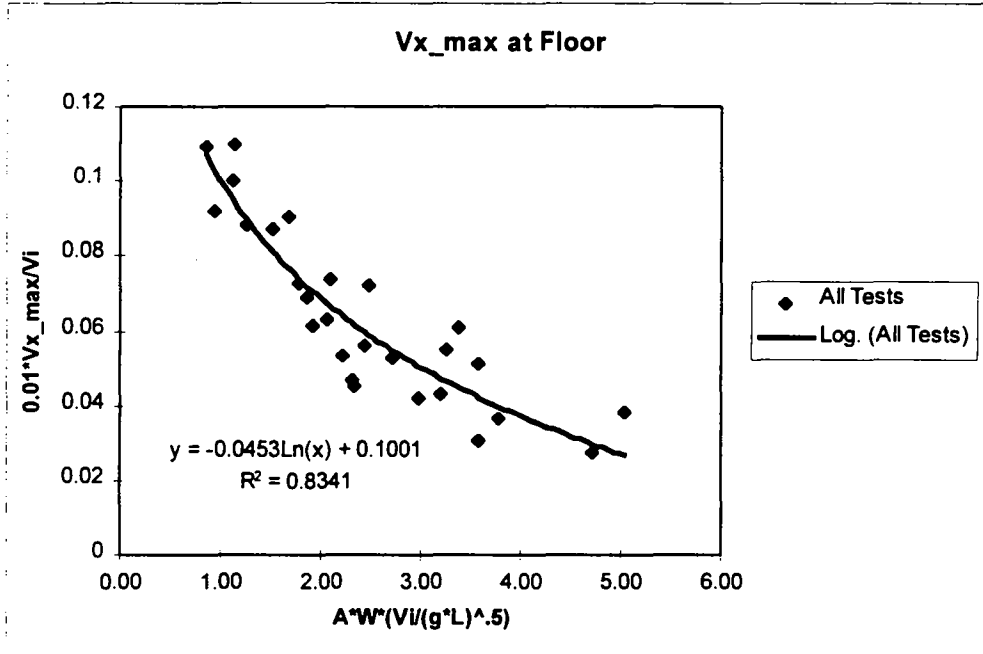


**Figure 4.15: Vx\_max at Floor**

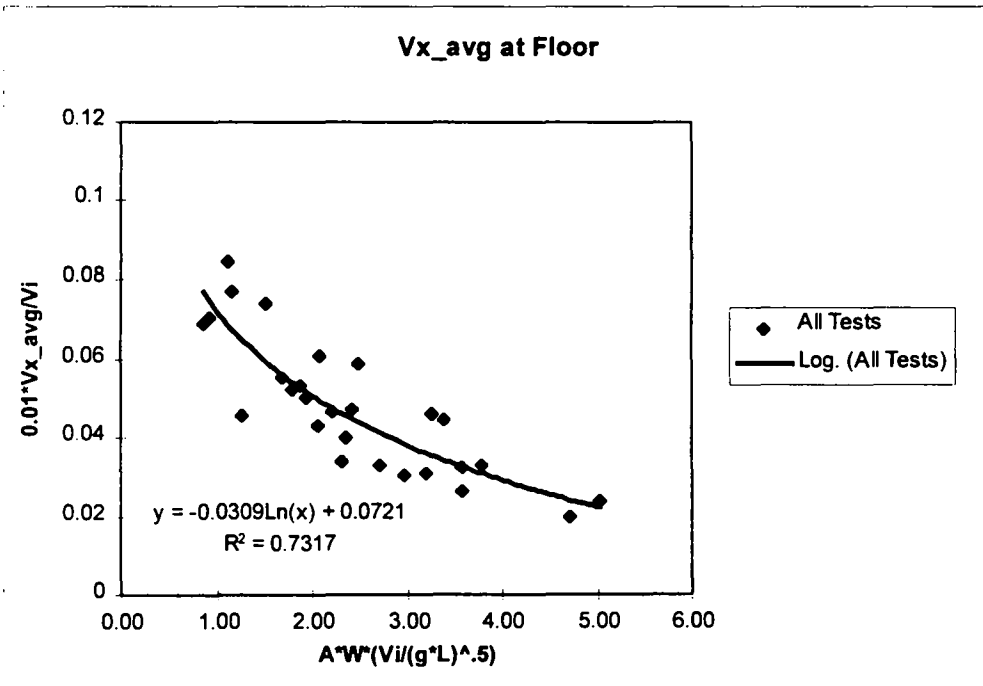


**Figure 4.16: Vx\_avg at Floor**

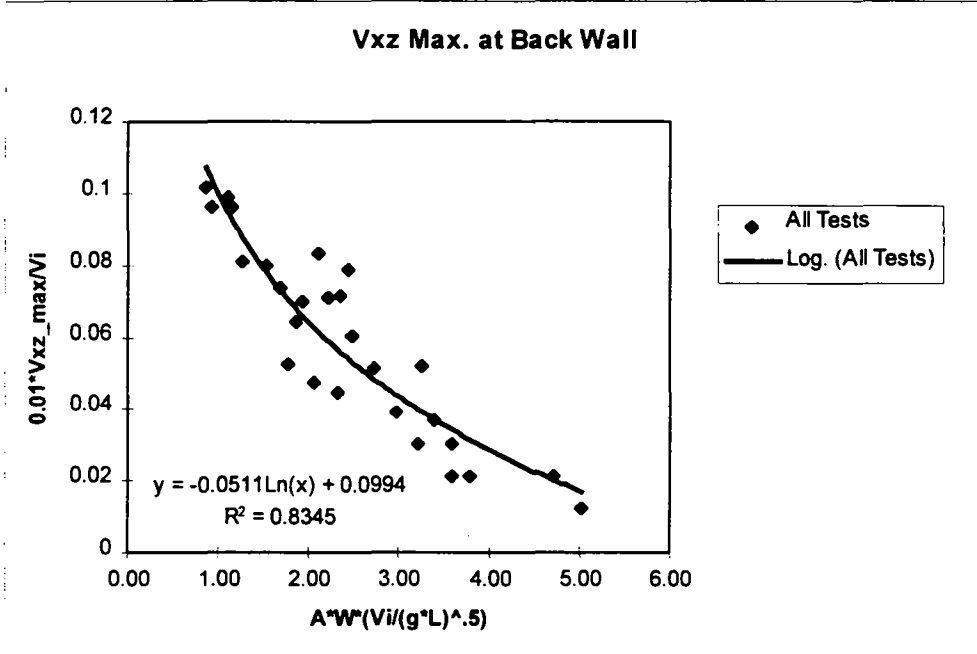


**Figure 4.17: Vxz Max. at Back Wall**

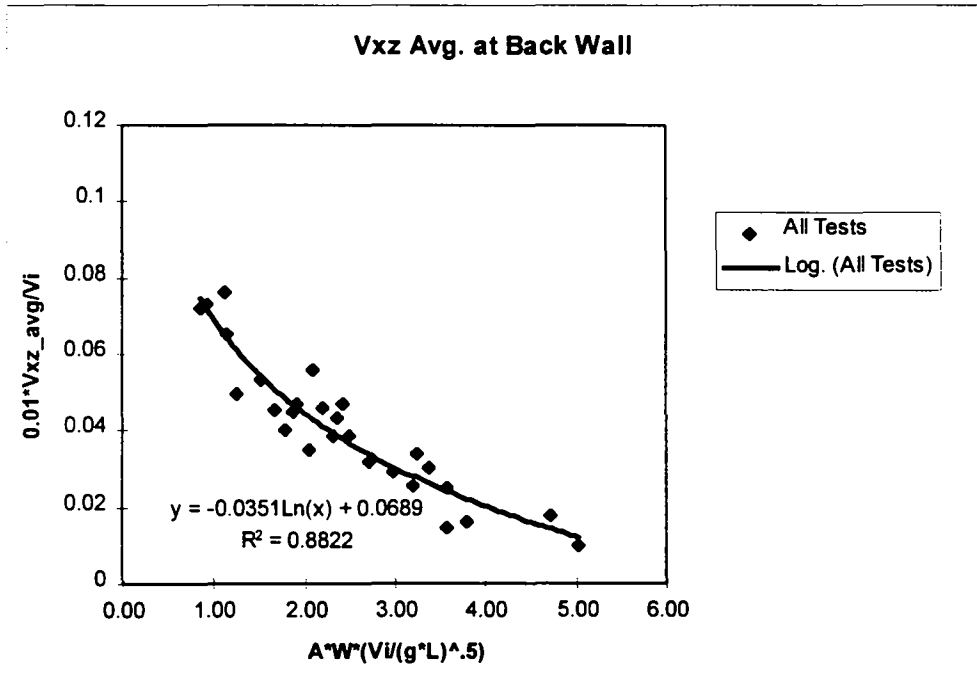


**Figure 4.18: Vxz Avg. at Back Wall**

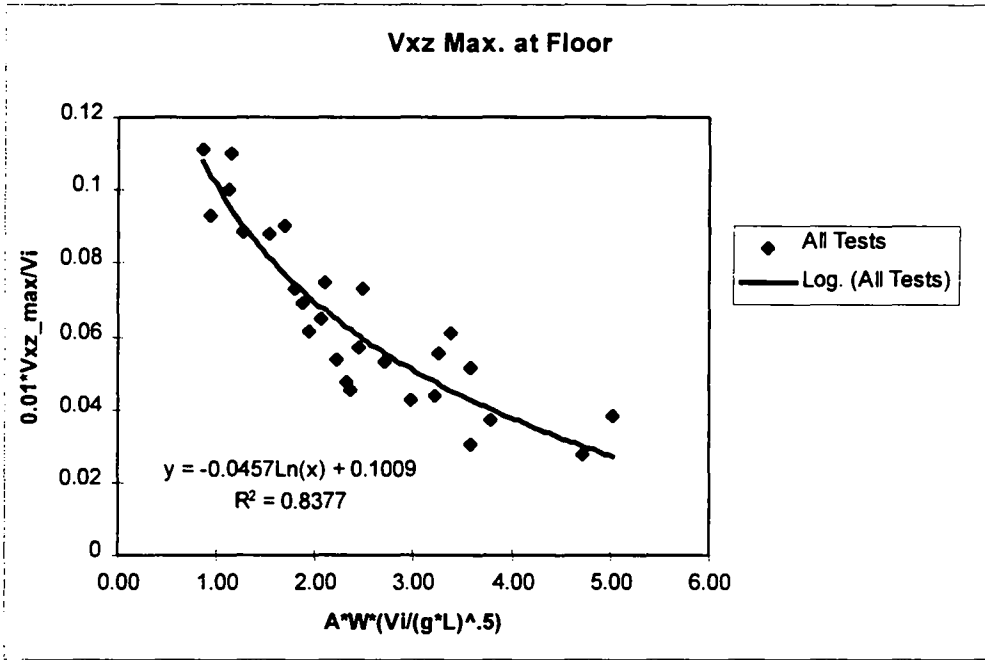


**Figure 4.19: Vxz Max. at Floor**

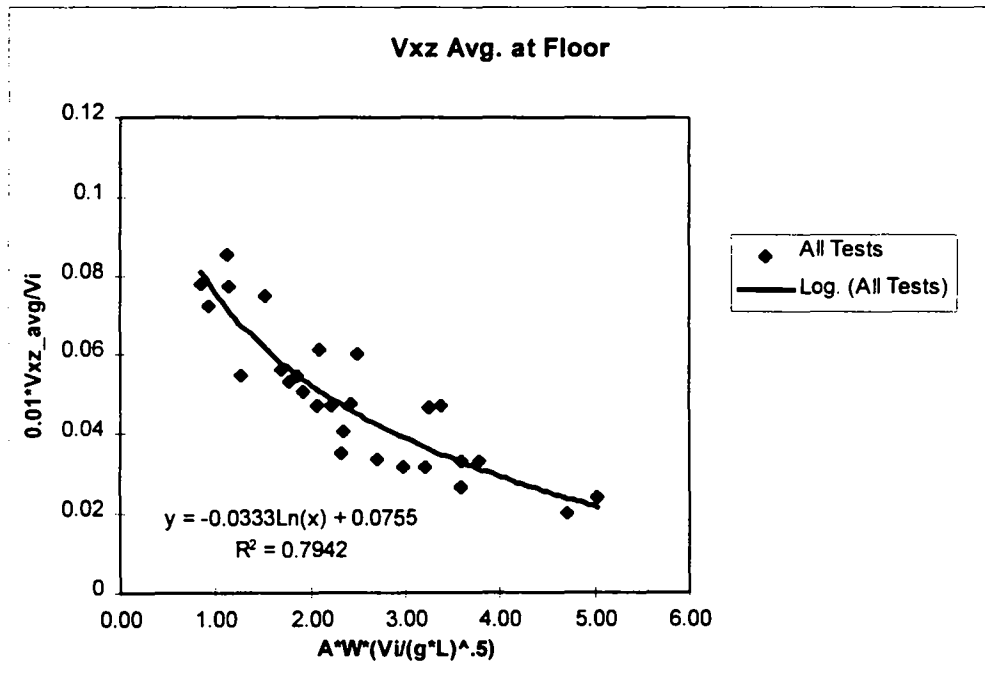


**Figure 4.20: Vxz Avg. at Floor**

The regression equations describing the data in Figure 4.13 through Figure 4.20 are of the form:

$$\Pi_2 = m * \ln(\Pi_1) + n \quad (4.3)$$

where

$$\Pi_1 = A * W * \frac{V_i}{\sqrt{g * L}}$$

$$\Pi_2 = \pm 0.01 * \frac{V^*}{V_i}$$

$m$  = dimensionless coefficient

$n$  = dimensionless coefficient

The regression equations are based on the results of all eighteen tests. The regression equation coefficients and coefficients of determination ( $R^2$ ) for each regression equation are summarized in Table 4.5.

**Table 4.5: Regression Coefficients and  $R^2$  Values**

Velocity Type	Zone	Velocity	Coefficients		$R^2$
			m	n	
Component	Back Wall	Vz_max	-0.0512	0.0982	0.8246
Component	Back Wall	Vz_avg	-0.0352	0.0678	0.8705
Component	Floor	Vx_max	-0.0453	0.1001	0.8341
Component	Floor	Vx_avg	-0.0309	0.0721	0.7317
Vector	Back Wall	Vxz_max	-0.0511	0.0994	0.8345
Vector	Back Wall	Vxz_avg	-0.0351	0.0689	0.8822
Vector	Floor	Vxz_max	-0.0457	0.1009	0.8377
Vector	Floor	Vxz_avg	-0.0333	0.0755	0.7942

The regression equations allow estimation of the velocity components and velocity vectors in the two critical zones within the roller region using the  $\Pi_1$  and  $\Pi_2$  parameters. Estimation of the velocity vectors will be slightly more accurate than estimation of the velocity components, as shown by the  $R^2$  values in Table 4.5.

#### 4.3.6 Velocity Comparisons

The velocities in the back wall zone are smaller in magnitude than the velocities in the floor zone, as presented in Table 4.6. The depth of the roller region is shorter in length than the distance between the upstream boundary and the upstream edge of the jet impact region. The shorter travel distance results in lost velocity potential because the flow does not have time to reach its full velocity potential due to flow pattern direction changes just above and just below the back wall zone.

**Table 4.6: Comparison of Back Wall Velocities to Floor Velocities**

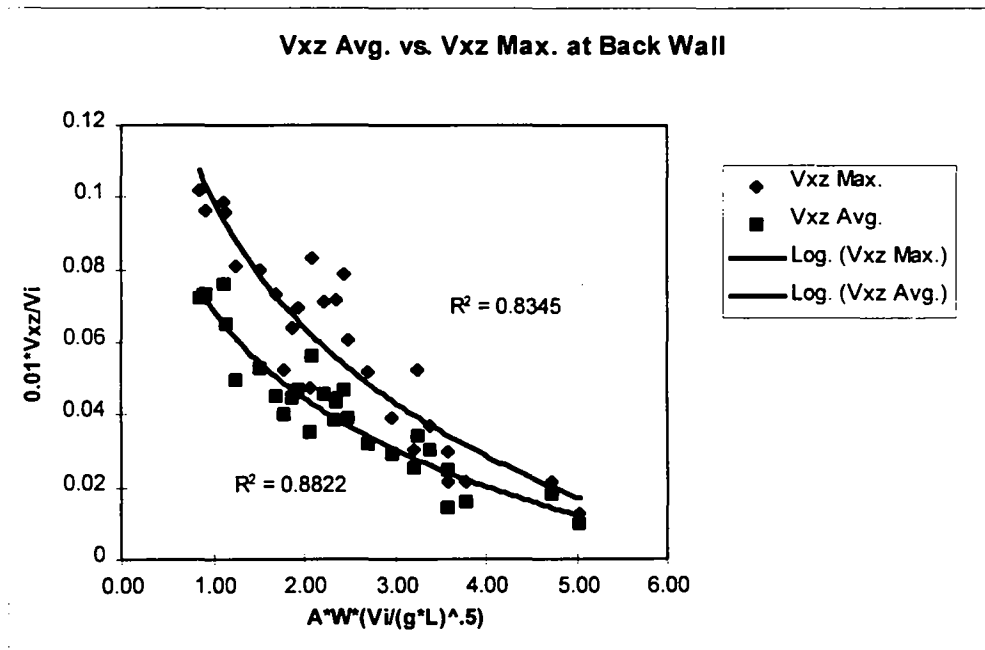
	Max. Values	Avg. Values
Back wall vector/Floor vector	89.54%	82.08%
Back wall major comp./Floor major comp	87.97%	82.11%

Figure 4.5 through Figure 4.12 illustrate the relationship between the average and maximum velocities. The ratios of average values to maximum values for velocity vectors and velocity components are presented in Table 4.7. Also included in Table 4.7 are the ratios of the velocities in the plunge pool basin to the impact velocity. The positive Z-direction is vertically upward, thus,  $V_{z\_min}$  is the maximum downward velocity.

**Table 4.7: Comparison of Average and Maximum Vectors and Components**

Back Wall Zone		Floor Zone	
Vector:	(%)	Vector:	(%)
Vxz_avg/Vxz_max	71.5%	Vxz_avg/Vxz_max	76.5%
Vxz_max/Vi	5.9%	Vxz_max/Vi	6.4%
Vxz_avg/Vi	4.1%	Vxz_avg/Vi	4.9%
Component:	(%)	Component:	(%)
Vz_avg/Vz_min	70.9%	Vx_avg/Vx_max	75.0%
Vz_min/Vi	5.7%	Vx_max/Vi	6.4%
Vz_avg/Vi	4.0%	Vx_avg/Vi	4.7%
Vx_avg/Vz_avg	10.8%	Vz_avg/Vx_avg	8.1%

Figure 4.21 and Figure 4.22 compare the maximum and average velocity vector data for the back wall and floor zones. Figure 4.21, Figure 4.22, and Table 4.7 demonstrate that in the back wall and floor zones, the ratios of the average velocity to the maximum velocity are between 70% and 75%.



**Figure 4.21: Vxz Max. and Avg. at Back Wall**

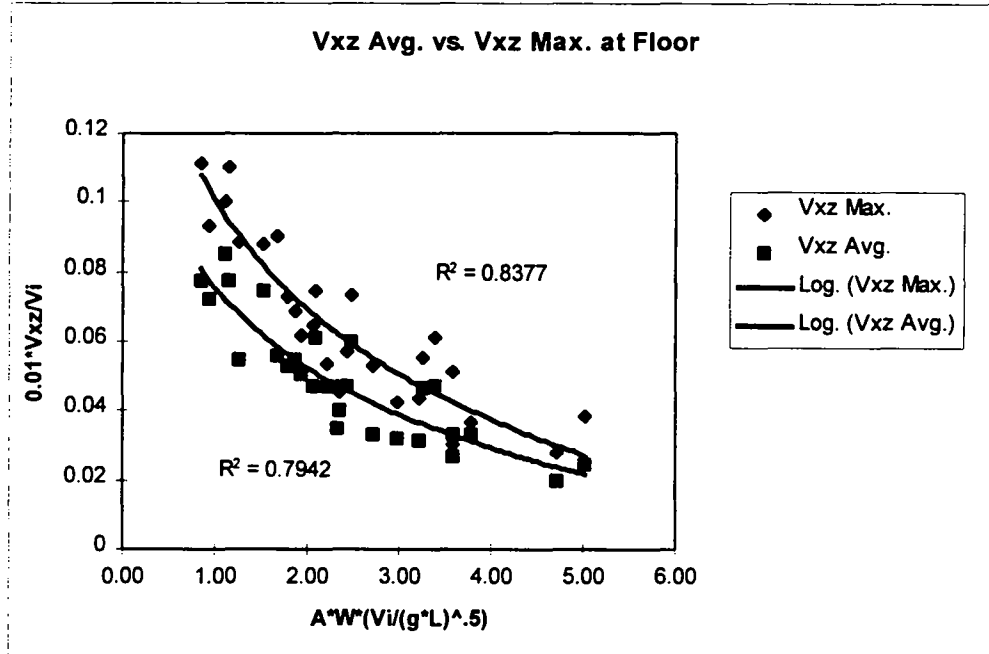


**Figure 4.22: Vxz Max. and Avg. at Floor**

The velocities in the back wall and floor zones are much smaller than the velocity at impact due to the high energy dissipation which occurs at impact with the surface and as the jet plunges into the plunge pool. The velocities in the circulation pattern in the plunge pool are an order of magnitude smaller than the impact velocity, as presented in Table 4.8. The maximum velocity vector and velocity component measured in the back wall and floor zones are also presented in Table 4.8

**Table 4.8: Maximum Velocities for All Tests**

	Max. Velocity/ $V_i$		Max. Velocity	
	Back Wall	Floor	Back Wall	Floor
	(%)	(%)	(cm/s)	(cm/s)
Vector	10.2%	11.1%	39.57	47.46
Component	10.1%	11.0%	38.91	47.35

The velocity vectors or velocity components in the either zone never exceeded 11.1% of the velocity at impact, as documented in Table 4.8.

#### 4.4 Spurious Correlation Analysis

The dimensionless groups  $\Pi_1$  and  $\Pi_2$  used for the regression analysis contain the same variable,  $V_i$ . Use of a common variable in both the dependent and independent variable groups on the axes of a regression plot can cause “spurious correlation” of the results. The result of spurious correlation is that the coefficients of determination may be greater in magnitude than those which occur without the use of a common variable. The advantage of using a common variable in both axes of the regression plots is that the groups remain dimensionless

An analysis of the spurious correlation was conducted. When the velocity data are plotted against a horizontal axis that excludes  $V_i$  from the horizontal axis, the data continues to be accurately described by natural log based regression equations. Figure 4.21 and Figure 4.22 use the dimensionless quantities on the axes; the corresponding figures using the dimensional horizontal axis which excludes  $V_i$  are presented in Appendix B. As shown in Table 4.9, on average approximately 13% of the coefficient of determination value is due to spurious correlation.

**Table 4.9: Spurious Correlation**

Location	Velocity	R <sup>2</sup> with Spurious Corr. Included	R <sup>2</sup> with Spurious Corr. Excluded	% R <sup>2</sup> due to Spurious Corr.
Back Wall	Vxz Max.	0.8345	0.7626	9%
Back Wall	Vxz Avg.	0.8822	0.7717	13%
Floor	Vxz Max.	0.8377	0.7172	14%
Floor	Vxz Avg.	0.7942	0.6631	17%

It was determined that documentation of the results of this research would incorporate the dimensionless groups and plots which include the common variable. The reasoning is threefold: inclusion or exclusion of the common variable does not change the type of equation which best describes the data (natural log based); the amount of spurious correlation present is relatively small; and using the dimensional group resulting from the exclusion of  $V_x$  from the horizontal axis would greatly inhibit the accuracy and applicability for scaling.

#### 4.5 Erosion Potential

Based on the velocities observed in the circulation pattern in the roller region, the potential for erosion due to the circulating flow is small. Using 47.46 cm/s (the maximum velocity vector measured for all tests) and the tailwater depths measured during testing, the Neill equation (Simons and Senturk, 1992) calculates that the largest sediment particle at incipient motion is 1.9 mm in diameter. Thus, the velocities in the circulation pattern produced under the model conditions have limited potential for transporting sediment from a dam foundation.

An impact prediction procedure (Bohrer, 1996) (see Chapter 5 for discussion) was used to model a full scale dam overtopping condition to determine the impact

2) Canyon Width / Jet Width ( $W$ ):

$W$  between 1.0 and 3.0

The zones of the plunge pool basin in the field at which the velocity prediction equations are applicable are as follows:

Dam face applicability zone boundaries:

X-direction: From the back wall to  $0.1 X_r$ ,

Y-direction: Zone width equals the jet width at impact

Z-direction:  $0.33 L$  to  $0.70 L$

Plunge pool floor applicability zone boundaries:

X-direction:  $0.33 X_r$  to  $0.70 X_r$ ,

Y-direction: Zone width equals the jet width at impact

Z-direction: From the floor to  $0.15 L$

where

$L$  = Depth in the roller region ( $L$ ) (Figure 4.4)

$X_r$  = Distance from upstream boundary to upstream side of jet at impact ( $L$ ) (Figure 4.4)

## 5.2 Implementing the Velocity Prediction Equations

In order to implement the velocity prediction equations, the following information as related to a specific overtopping condition is required:

- Jet impact velocity,  $V_j$  (section 5.2.1)
- Jet impact air concentration,  $A$  (section 5.2.2)
- Ratio of canyon width to jet width,  $W$  (measured in field)
- Tailwater depth in the plunge pool,  $L$  (see discussion below)

The tailwater depth in the plunge pool is to be calculated using standard backwater profile techniques for the existing canyon geometry downstream of the dam and for the total expected discharge. The coefficients presented in Table 4.5 are used

to yield the velocity prediction equation for the desired velocity,  $V$  (velocity component, velocity vector, maximum value, average value, etc.), at the desired zone (dam face or plunge pool floor). In order to determine the desired velocity in the circulation pattern at the desired location, the procedure is as follows:

- 1) Obtain  $V_i$ ,  $A$ ,  $W$ , and  $L$  and input into Equation 4.1:

$$\Pi_1 = A * W * \frac{V_i}{\sqrt{g * L}} \quad (4.1)$$

- 2) Solve Equation 4.1 for  $\Pi_1$
- 3) Input  $\Pi_1$  and the appropriate coefficients  $m$  and  $n$  from Table 4.5 into Equation 4.3:

$$\Pi_2 = m * \ln(\Pi_1) + n \quad (4.3)$$

- 4) Solve Equation 4.3 for  $\Pi_2$
- 5) Input  $\Pi_2$  and  $V_i$  into Equation 4.2:

$$\Pi_2 = \pm 0.01 * \frac{V}{V_i} \quad (4.2)$$

- 6) Solve for  $V$

When calculating values in Equation 4.2,  $V$  must have units of cm/s, while  $V_i$  must have units of m/s. If  $V$  is the downward velocity component in the Z-direction, the sign on the right hand side of Equation 4.2 is negative. If  $V$  is a velocity component in the X-direction or a velocity vector, the sign on the right hand side of Equation 4.2 is positive.

It is advised that when performing predictive calculations, the maximum velocity vector prediction equations be used as opposed to the velocity component prediction

velocity at the plunge pool surface. Using a dam with a crest width of 15 m discharging 100 m<sup>3</sup>/s with a drop height of 24 m, the resulting impact velocity is 5.48 m/s (Bohrer, 1996). The maximum velocities in the circulation pattern in the roller region will be approximately 11% of the impact velocity. Thus, the maximum velocities in the plunge pool will be approximately 0.60 m/s. Using the Neill equation with a velocity of 0.60 m/s, the largest diameter particle that will be transported (for various depths) are shown in Table 4.10.

**Table 4.10: Sediment Transport Capabilities, Field Condition**

Depth	Largest Particle at Incipient Motion
(m)	(mm)
1	4.9
3	3.8
6	3.2
10	2.8

In order for dam failure to occur, a large amount of sediment must be removed from the dam foundation. Thus, for both the model condition and field condition, the velocities in the plunge pool are relatively low with a limited capacity to mobilize soil particles.

## CHAPTER 5

### VELOCITY PREDICTION PROCEDURE

A velocity prediction procedure for determining circulation velocities at the upstream boundary and the plunge pool was developed. Maximum and average velocity prediction equations were developed for X-direction and Z-direction velocity components and XZ-plane velocity vectors. The velocity prediction equations are based upon dimensionless quantities.

#### 5.1 Applicability

The back wall and floor zones in the model are representative of the downstream dam face and the plunge pool floor in a field situation. The prediction equations allow prediction of the magnitude and direction of circulation velocities along the downstream dam face and along the base of the plunge pool upstream of the jet impact location. In order to apply the prediction equations developed herein to a field situation, the jet in the field must be rectangular, free falling, developed, and impact the free surface of the plunge pool. Also, the relative dimensions of the field geometry should be similar to the those used to develop the prediction equations. The field geometry dimensions must meet the following criteria:

- 1) Tailwater Depth / Drop Height ( $L_d/H$ ):

$L_d/H$  between 0.26 and 0.85

equations. The recommended maximum velocity vector prediction equations for the dam face and plunge pool base zones are:

Dam face (Back wall zone):

$$\Pi_2 = -0.0511 * \ln(\Pi_1) + 0.0994 \quad (5.1)$$

Plunge pool floor (Floor zone):

$$\Pi_2 = -0.0457 * \ln(\Pi_1) + 0.1009 \quad (5.2)$$

The recommended form of Equation 4.2 is:

$$\Pi_2 = 0.01 * \frac{V_{xz\_max}}{V_i} \quad (5.3)$$

Impact velocity and air concentration estimates for a rectangular, developed free falling jet may be calculated using the equations developed by Lewis (1996) and Bohrer (1996).

### 5.2.1 Impact Velocity

Bohrer (1996) refined the impact velocity estimation procedure for a developed, rectangular, free falling jet developed by Lewis (1996). The resulting iterative procedure uses the following equations:

For  $j = 1, 2, \dots, \frac{H}{\Delta H}$ :

$$V_j = \sqrt{V_{j-1}^2 + 2g\Delta H} - 3C_d \left( \frac{\rho_a}{\rho_w} \right) \left( \frac{\Delta H}{d} \right) V_{ave_j} \quad (5.4)$$

$$V_{ave_j} = \frac{V_{j-1} + \sqrt{V_{j-1}^2 + 2g\Delta H}}{2} \quad (5.5)$$

$$V_i = V_{\frac{H}{\Delta H}} - C_i \quad (5.6)$$

where

- $H$  = Drop height (L)
- $\Delta H$  = Incremental length of the drop height (constant) (L)
- $V_j$  = Velocity at the end of the  $j$ th incremental length (L/T)
- $V_{j-1}$  = Velocity at the beginning of the  $j$ th incremental length (L/T)
- $V_{ave_j}$  = Estimated average velocity using the beginning and end velocities of the  $j$ th incremental length (L/T)
- $V_{\frac{H}{\Delta H}}$  = Velocity at the end of the  $\frac{H}{\Delta H}$  th incremental length (L/T)
- $V_i$  = Impact Velocity (L/T)
- $C_i$  = Impact velocity constant (L/T)
- $C_d$  = Drag coefficient
- $\rho_a$  = Air density (M/L<sup>3</sup>)
- $\rho_w$  = Water density (M/L<sup>3</sup>)
- $g$  = Gravitational acceleration (L/T<sup>2</sup>)
- $d$  = Diameter of sphere having the same volume as a water drop (L)

The Visual Basic<sup>®</sup> program code used to solve the iterative procedure is presented in Appendix A.

### 5.2.2 Impact Air Concentration

Bohrer (1996) developed a dimensionless air concentration at impact estimation equation for a developed, rectangular free falling jet as follows:

$$\text{Impact air conc. \%} = 12.286 * \ln\left(\frac{V_o^2 * H}{g * A}\right) + 17.535 \quad (5.7)$$

where

- $V_o$  = Issuance velocity (L/T)
- $H$  = Drop height (L)
- $A$  = Area of jet at issuance (L<sup>2</sup>)
- $g$  = Gravitational acceleration (L/T<sup>2</sup>)

## CHAPTER 6

### CONCLUSIONS & RECOMMENDATIONS

The goals of the study were to determine the flow patterns in the plunge pool basin upstream of the jet impact location, enhance understanding of the driving forces producing the flow patterns, and develop a procedure to predict the flow velocities at the downstream dam face and plunge pool floor in the plunge pool stilling basin. The study included a review of related literature, construction of a hydraulic model of an overtopping dam, conducting eighteen tests varying discharge, tailwater depth, and basin width, formulating dimensionless groups which describe the flow characteristics, analyzing the test data, and developing a velocity prediction procedure for the downstream dam face and floor zones of a plunge pool stilling basin.

#### 6.1 Conclusions

The following conclusions are drawn from the results of the project:

- Circulation direction in the roller region is counter-clockwise (downstream flow is left to right) and remained consistent for all testing conditions (Figure 4.1).

The direction of the circulation pattern is contrary to previous perceptions (Cola, 1965, Jirka and Harleman, 1979).

- The flow patterns result from a combination of driving forces:

1. Rebound effect of the plunging jet off of the stagnation point (when diffusion of the jet has not completely occurred in the plunge pool prior to impact with the stagnation point),
  2. Upward buoyancy force due to the high amount of air entrainment in the plunging jet, and
  3. Horizontal spreading force of the jet due to impact with the water surface.
- The velocities in the roller region are a function of the jet velocity at impact, jet air concentration at impact, jet width, basin width, tailwater depth, and gravitational acceleration.
  - As the canyon width decreases, the circulation velocities in the roller region increase.
  - The magnitude of the velocities along the back wall are approximately 80% of the magnitude of the velocities along the floor.
  - The magnitude of the average velocity components and vectors are 70% to 75% of the magnitude of the maximum velocity components and vectors.
  - The magnitude of the velocities in the circulation pattern of the roller region are an order of magnitude smaller than the impact velocity.
  - The velocities in the roller region can be predicted using the velocity prediction equations (Equation 4.1 through Equation 4.3) developed for maximum and average velocity components or maximum and average velocity vectors.

- The circulating flow in the roller region has a limited erosion and sediment transport capacity.

## 6.2 Recommendations

The Plunge Pool Circulation and Velocity Prediction study addressed a variety of complex issues. Further research in the following areas would be very beneficial:

- Determine the effect varying the distance between the upstream boundary and jet impact location has on flow patterns and velocities in the roller region.
- Establish the effect varying the angle of jet issuance has on flow patterns and velocities in the roller region to determine the applicability of this research to flip bucket discharge.
- Conduct tests on prototype model and compare scaled results.
- Expand the prediction equations outside the applicability ranges.

## REFERENCES

- Albertson, M.L., Dai, Y. B., Jensen, R. A., and Rouse, H. (1950). Diffusion of Submerged Jets. *Proc. of A.S.C.E.*, Vol. 115, No. 2409.
- Beltaos, S., (1976). Oblique Impingement of Plane Turbulent Jets. *Journal of the Hydraulics Division, A.S.C.E.*, Vol. 10, No. HY9, 1177-1192.
- Beltaos, S. and Rajaratnam, N., (1973). Plane Turbulent Impinging Jets. *Journal of Hydraulic Research.*, Vol. 11 No 1.
- Bohrer, J. G., (1996). Plunge Pool Velocity Prediction of Jets Formed by Overtopping Steep Dams. *M. S. Thesis*, Colorado State University, Ft. Collins, Colorado.
- Breusers, H. N. C., (1991). Scour by Jets, at High-Head Structures and at Culvert Outlets. *Hydraulic Structures Design Manual*, Vol. 2.
- Cola, R., (1965). Energy Dissipation of a High Velocity Vertical Jet Entering a Basin. *Inter. Assc. Hydr. Res. - Proceedings.*, 11th Congress, Vol. 1, paper no. 1.52.
- Ervine, D. A., and Falvey, H. T., March (1987). Behavior of Turbulent Water Jets in the Atmosphere and in Plunge Pools. *Proceedings of the Institution of Civil Engineers*, Part 2, Vol. 83.
- Frizell, Kathleen H., Ehler, David G., and Mefford, Brent W., (1994). Developing Air Concentration and Velocity Probes for Measuring Highly Aerated, High-Velocity Flow. *Fundamentals and Advancements in Hydraulic Measurements and Experimentation*, A.S.C.E.
- George, R.L., (1980). Impinging Jets. *Engineering and Resource Center, Water and Power Resources Service*, No. REC-ERC-80-8.
- Iamandi, C. And Rouse, H., (1969). Jet-Induced Circulation and Diffusion. *Journal of the Hydraulics Division, Proc. A.S.C.E.*, Vol. 95 (HY2), 589-601.
- Jirka, G. H. And Harleman, D., (1979). Stability and Mixing of a Vertical Plane Buoyant Jet in Confined Depth. *Journal of Fluid Mechanics*, Vol. 92, Part 2, 275-304.

- Lee, J. and Jirka, G. H., (1981). Vertical Round Buoyant Jet in Shallow Water. *Journal of the Hydraulics Division.*, Vol. 107 No HY12, 1651-1675.
- Lewis, T. L., (1996). Prediction of Velocities Within Jets Formed By Overtopping Steep Dams. *M.S. Thesis.*, Colorado State University, Ft. Collins, Colorado.
- Lohrmann, A., Cabrera, R., and Kraus, N.C., (1994). Acoustic-Doppler Velocimeter (ADV) for Laboratory Use. *Fundamentals and Advancements in hydraulic Measurements and Experimentation*, ASCE.
- Marsh-McBirney, Inc., (1985). Model 201 Portable Flow Meter.
- Simons, D. B. and Senturk, F. (1992). *Sediment Transport Technology - Water and Sediment Dynamics*. Littleton, Colorado: Water Resources Publications.
- Stearns, R. F., Johnson, R.R., Jackson, R.M., and Larson, C.A., (1951). *Flow Measurement with Orifice Meters*, D. Van Nostrand Company, Inc.

## APPENDIX A

### PROGRAM CODE: IMPACT VELOCITY ESTIMATION (Bohrer, 1996)

Function theory(V, H, CD, D)

D = D / 1000

vold =  $(V^2 + 2 * 9.81 * 0.001)^{0.5} - (3 * CD * 0.00112 * 0.001 / D * (V + \sqrt{V^2 + 2 * 9.81 * 0.001}) / 2)$

x = 0.002

Do Until x >= H

vnew =  $(vold^2 + 2 * 9.81 * 0.001)^{0.5} - (3 * CD * 0.00112 * 0.001 / D * (vold + \sqrt{vold^2 + 2 * 9.81 * 0.001}) / 2)$

vold = vnew

x = x + 0.001

Loop

theory = vold - 0.5

End Function

Program variable definitions:

V = Issuance Velocity (m/s)  
H = Drop Height (m)  
CD = Drag Coefficient  
D = Droplet Diameter (mm)

Note typical variable values documented by Bohrer (1996):

CD = 0.49  
D = 6.00 mm

## APPENDIX B

### PLOTS EXCLUDING SPURIOUS CORRELATION

